Evaluation of different approaches for the estimation of the seismic vulnerability of masonry towers

Vasilis Sarhosis[(1)], Gabriele Milani[(2)*], Antonio Formisano[(3)], Francesco Fabbrocino[(4)]

(1) University of Newcastle, Newcastle, UK
(2) Technical University of Milan, Milan, Italy
(3) University of Naples Federico II, Naples, Italy
(4) University Pegaso, Naples, Italy

Abstract

A series of simplified approaches are evaluated for their effectiveness to estimate the seismic vulnerability of historic masonry towers. First, collapse loads are evaluated on sixteen "idealized" benchmark cases with different slenderness and shear area. Both analytical and computational approaches are used, namely the analytical procedure proposed by the Italian Guidelines on the Built Heritage and pushover analyses conducted using the commercial codes UDEC and 3Muri. The sixteen towers are representative cases which can be encountered in practice. Their geometry is idealized into parallelepiped blocks with hollow square cross-sections, thus favoring the utilization of 2D approaches, beneficial to drastically reduce the effort required for repeated computations. In addition, a Monte Carlo MC upper bound limit analysis strategy is proposed, in order to have an insight into the possible failure mechanisms for the different cases investigated. Deliberately is avoided the introduction of any form of irregularity and they are supposed isolated from the neighboring buildings, to obtain results exclusively dependent from geometric features. Among all the possible collapse mechanisms, five of them are selected according to the probability of occurrence based on past earthquake experiences. Five million cloud points of collapse accelerations are obtained by carrying the height, slenderness and shear area of the idealized towers. The approach is very fast and allows identifying different regions where single mechanisms are active. The results are confirmed repeating MC simulations with a triangular FE upper bound limit analysis discretization of the idealized towers. A series of equations are provided in order to assist engineers and practitioners to obtain a preliminary estimation of their expected collapse acceleration. For validation purposes, the results obtained previously with refined full 3D FE models of 25 towers located in the Northern Italy are reported. Satisfactory agreement between the predictions provided by simplified methods and sophisticated analyses are obtained.

Keywords: masonry; towers; seismic vulnerability; UDEC; 3Muri; limit analysis

*** Corresponding author:** Prof Gabriele Milani, Technical University of Milan, Department ABC, Piazza Leonardo da Vinci 32, 20133 Milan, Italy e-mail: gabriele.milani@polimi.it

1 Introduction

The preservation of the architectural heritage is a task of great societal importance for developed countries in Europe and technically a very challenging aim, especially in seismic areas. Masonry towers in form of medieval defense structures as well as clock and bell towers in churches are quite diffused all over Europe and are an important part of the historical and architectural heritage to be preserved. Recent seismic events have highlighted that ancient masonry towers are particularly susceptible to damage and prone to partial or total collapses under earthquake excitations. The safety assessment of such unique masterpieces against horizontal loads is therefore paramount and this paper deals with such particular topic. Old masonry towers usually show peculiar morphologic and typological characteristics which are at the base of all the difficulties encountered in the recent past to find a standardized methodology to predict their behavior under horizontal loads and hence give a reliable safety assessment.

In ancient times, towers were exclusively conceived to be able to withstand vertical loads. Recently, however, national and international standards (e.g. NTC 2008; Circolare N617 2009; DPCM 2011; EC8 2005) have imposed the evaluation of the structural performance in presence of horizontal loads, which simulate earthquake excitations, encouraging the use of sophisticated non-linear methods of analysis. According to the previous remarks, it is pretty clear that the most accurate approach to deal with the analysis of masonry towers under horizontal loads should require specific ad hoc FE approaches (Curti el al. 2006; Carpinteri et al. 2006; Riva et al. 1998; Bernardeschi et al. 2004; Pena et al. 2010; Bayraktar et al 2010; Milani et al 2012a; Milani et al. 2012b; Casolo et al. 2013; Acito et al. 2014; Valente & Milani 2016a, 2016b, 2017; Milani et al. 2017) in order to deal with the complexity of the problem through a suitable level of accuracy.

However, in engineering practice, the utilization of non-linear methods and full 3D Finite Element models is not so common, because commercial codes with advanced material models should be adopted by users that are supposed to have a strong mathematical and mechanical background and deep knowledge on sophisticated non-linear analyses conducted with FEs.

To cope with this key issue, the Italian code for the built heritage (DPCM 2011) allows evaluating the seismic vulnerability of masonry towers by means of a simple cantilever beam approach, where only flexural failure is taken into consideration. Such procedure is very straightforward and can be tackled even by unexperienced practitioners without the need of using any advanced computational methods of analysis such as FE codes. The drawback is represented by the impossibility to account for a combined shear and flexural failure of the towers, which in practice is common in case of low slenderness.

In order to put at disposal to practitioners some formulas to preliminarily estimate the seismic vulnerability of an existing tower (without the need to perform any calculation), in the present paper we analyze a series of “idealized” benchmark cases using different simplified approaches, namely the procedure proposed by the Italian code and pushover conducted with two commercial codes (UDEC and 3Muri). The geometry is intentionally idealized into parallelepiped blocks with hollow square cross-section, favoring the utilization of 2D approaches, in order to drastically reduce the computational effort required in carrying out medium scale systematic computations and avoiding the introduction of any kind of irregularity, such as presence of a bell cell, openings, internal vaults etc. Also, the variation of thickness along the height, which is a very common feature for slender towers, falls within the wide case of “geometric irregularities” and is preliminary disregarded in this study to limit the high number of possibilities that can be encountered in reality. Intentionally with the aim of furnishing results exclusively related to their own geometric features, towers are also assumed isolated from the neighboring structures. Obviously, such hypothesis represents a strong limitation, because towers are often connected to adjacent structures (the church, in the case of bell towers; the city walls or other buildings in aggregate, in the case of civic towers), and will be removed

in a dedicated research, where both irregularities and interaction with neighboring buildings will be dealt with parametrically. Within the present simplified framework, 16 different cases that can be encountered in practice are critically discussed, changing three key parameters that proved to be important for the vulnerability determination, namely height, slenderness and transversal shear area.

The simplifications introduced in the modelling phase allow for fast sensitivity analyses in the inelastic range and an estimation of the vulnerability in that range of slenderness that is useful for practical purposes. Simplified formulas fairly representing the obtained seismic vulnerability are also reported and put at disposal to any practitioner interested in a preliminary estimation of the behavior of the towers before doing any calculation.

Then, a Monte Carlo (MC) upper bound limit analysis strategy is proposed, in order to have an insight into the possible failure mechanisms active in the different cases. Among all the possible collapse mechanisms, five (the most meaningful) are selected in light of the experience of collapses deriving from post-earthquake surveys. These are: (a) vertical splitting into two parts, (b) base rocking, (c) overturning with diagonal cracks (Heyman 1995; Como 2013), (d) a combination of splitting and diagonal overturning; and (e) base sliding. In the framework of the upper bound theorem of limit analysis, the real mechanism is the one associated to the minimum multiplier and, being the possibilities reduced to only 5 options, large scale MC simulations can be performed changing height, slenderness and shear area of the idealized towers. Hence, 5 million cloud points of collapse accelerations are obtained, allowing the identification of clearly defined regions where single mechanisms are active, as a function of slenderness, shear area and height. The results are substantially confirmed repeating MC simulations with a triangular FE upper bound limit analysis discretization of the idealized towers, which roughly provided very similar outcomes. For validation purposes, the results obtained previously by one of the authors (Valente & Milani 2016a, 2016b, 2017) by means of refined full 3D Abaqus discretization of 25 towers located in the Northern Italy are finally reported. Good agreement between the predictions provided by the simplified methods here proposed and previously presented reference data is obtained.

2 The sensitivity analysis conducted

The sensitivity analysis conducted in the present paper is aimed at covering the majority of the real cases that can be encountered in practice. It relies into the investigation of the structural behavior of 16 “ideal” masonry towers, with different geometric features, such as a variety of heights, thicknesses and transversal cross sections, as illustrated in Figure 1. Intentionally, the ideal towers do not exhibit any form of irregularity, such as changes of thickness of the perimeter walls, presence of perforations of any kind (doors, windows, bell cells, etc.) and internal walls, stairs or vaults. The aim is indeed to simplify the approach to a great extent, in order to provide results in terms of seismic vulnerability that are dependent on only two geometric parameters, namely slenderness and cross shear area.

Table 1: Initial survey conducted in different Italian regions to investigate the typical geometrical features most diffused in the national territory

REGION	B1[(1)] (m)	B2[(1)] (m)	H (m)	t (cm)	λ	$\tilde{A}_s$
	Base edge length	**Base edge length**	**Height**	**thickness**	**Slenderness min-max**	**Shear area min-max**
Abruzzo	4–10	4–10	20–50	130–150	2-6	0.4-0.90
Campania	6–13	5–13	30–75	60–100	2.5-8	0.35-0.80
Emilia-Romagna	2–12	2–12	16-87	45-160	3-8.5	0.28-0.85
Marche	2.50-9	2.50-8	16-45	60-120	1.5-8	0.25-0.82
Molise	5-6.50	5-7	20-35	100-200	2-6	0.30-0.90
Toscana	5-10	6-10	27-55	130-260	2-9	0.35-0.85
Veneto	4-15	4-14	20-58	80-200	3-7	0.28-0.85
(1) In the present computations it is assumed B1=B2=B						

A preliminary work recently carried out at the University of Naples Federico II and partially presented in Formisano et al. (2017), deals with the geometric survey of several existing towers in 7 Italian regions. Among other information, the survey reports as final result the typical ranges of variability of the height, base width and wall thickness of existing towers that can be found in Italy. A concise synopsis is provided in Table 1. Ideal towers analyzed in this paper turn out to exhibit slenderness λ and normalized shear area $\tilde{A}_s$ (defined respectively as λ =H/B and $\tilde{A}_s = \left[B^2 - (B - 2t)^2 \right] / B^2$ as depicted in Figure 2, where also minimum and maximum values of λ and $\tilde{A}_s$ found during the survey are represented with green circles. From Figure 2, the ideal towers seem to fit well the general geometric characteristics of the real towers surveyed, meaning that they can be used to have a rough prediction of real cases under seismic loads. Each ideal tower is represented with its own symbol, differing in shape and color, so towers having small $\tilde{A}_s$s are depicted with cold colors (i.e. blue and cyan), whereas those with large $\tilde{A}_s$s with cool colors (i.e. yellow and red). Different values for λ s are represented with different symbols, namely squares, triangles, circles and diamonds. Each tower belonging to the same series (denoted with A, B, C and D) is characterized by the same $\tilde{A}_s$.

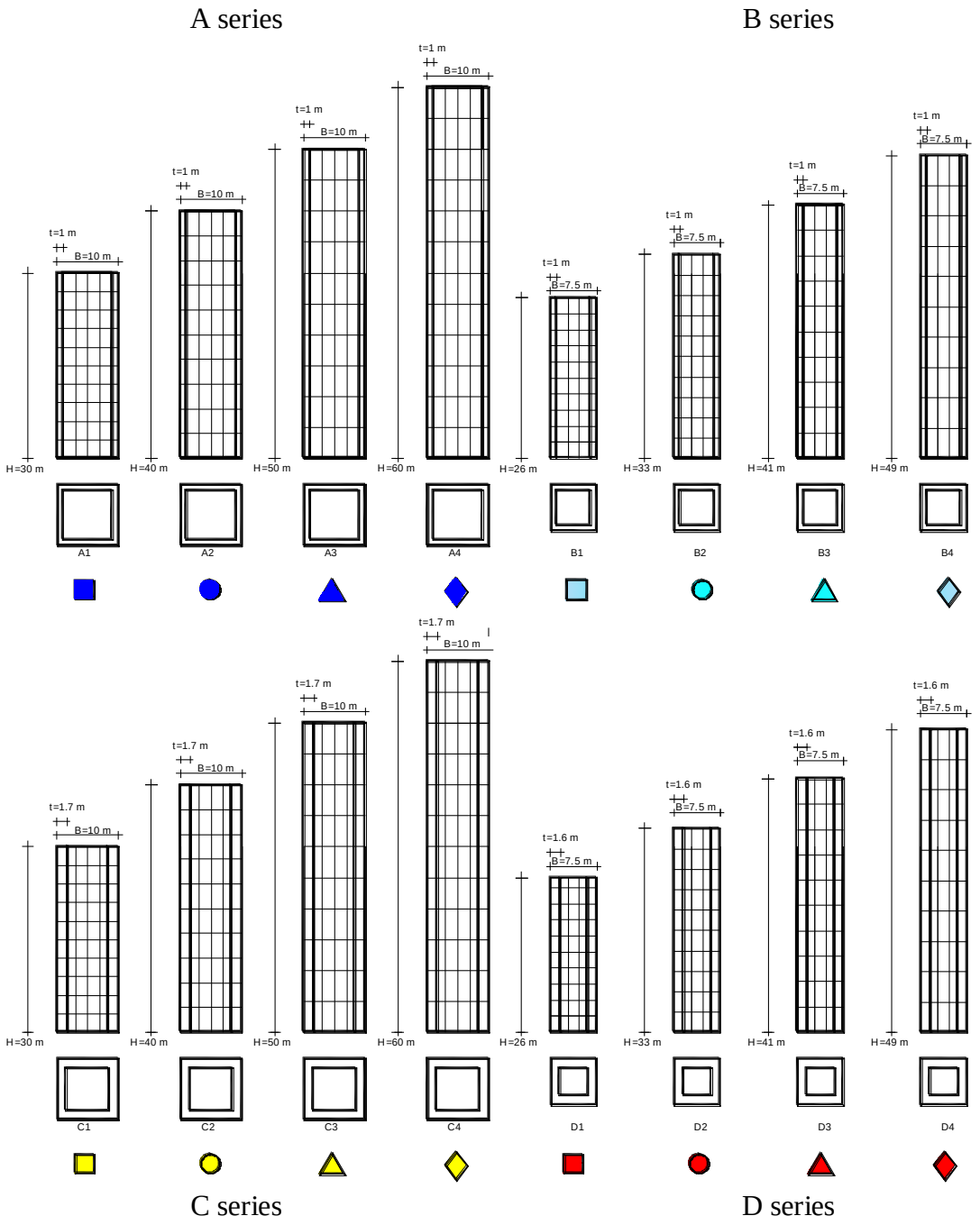

Figure 1: Geometric properties of the "ideal" case studies analyzed in the present paper. Each tower is labeled with a different symbol. Warm colors indicate large equivalent shear cross areas (>0.5), whereas cold colors indicate small equivalent cross areas.

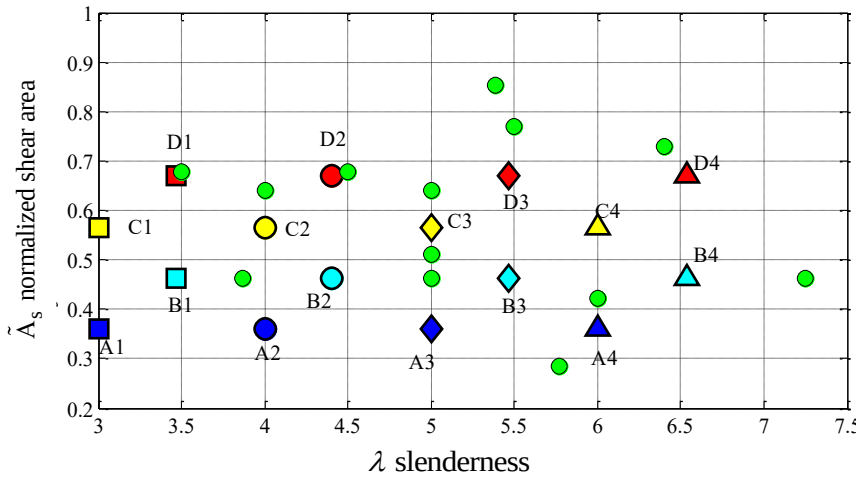

Figure 2: Relation between normalized shear cross area and slenderness for the different "ideal" towers analyzed for comparison purposes (green circles represent maximum and minimum values in different Italian regions, according to a survey made by the authors).

3 Methodology of evaluation of collapse accelerations and seismic vulnerability

In order to obtain the seismic vulnerability of the tower, three different approaches were utilized. These are: 1) the simplified approach according to Italian code (also known as Equivalent Static Analysis, ESA); 2) a push over analysis carried out using the UDEC software based on the distinct element method; and 3) a pushover analysis using the 3Muri software based on the finite element method.

3.1 Italian code specifics, Equivalent Static Analyses (ESAs)

According to the Italian Guidelines for the built heritage, equivalent static analyses (ESAs) should be carried out to estimate the seismic vulnerability of a masonry tower. They are conducted according to § 5.4.4 of the Guidelines (DPCM 2011)0, subdividing the tower in blocks with horizontal cross sections and adopting a distribution of horizontal forces on the blocks proportional to the product $W_i z_i$, being W_i the weight associated to the i-th block and z_i the vertical position of its center of mass. When evaluating the resultant horizontal force as $F_h = 0.85\ S_e(T_1)\ W/(qg)$, reference is made to an elastic response spectrum S_e reduced by the behavior factor q equals to 3.6 suggested by the above Guidelines in the case of geometry and mass regularity along the height. The spectral ordinate corresponding to the fundamental period T_1 is referred to a given spectrum, which can be either obtained from the Italian code (NTC 2008) or from EC8 (2005).

The fundamental period T_1 can be evaluated rigorously in this case using the well-known results on vibration of Euler-Bernoulli beams, or either using FEs or through empirical procedures (Fabbrocino 2016) for real cases. In particular, the frequency assuming a cantilever beam hypothesis is given by the following simple formula:

$$f_i = \frac{\alpha_i}{2\pi L^2}\sqrt{\frac{EI}{\mu A}} \qquad (1)$$

Where μ is the density of the structure, E is the Young modulus, A and I the cross sectional area and inertia moment accordingly, L the height and α_i is a constant and is equal to 3.5156.

According to the Italian Guidelines, it is necessary to compare the acting bending moments on different transversal sections, within the application of equivalent static loads and under the hypotheses of class use and soil done, with the resisting ones.

For towers with rectangular section, FEM may be avoided and simplified formulas could be adopted according to Italian Guidelines specifics (NTC 2008). Under the hypothesis that the normal pre-compression does not exceed $0.85\,f_d\,A$, the ultimate bending moment of a masonry rectangular sections is:

$$M_u = \frac{\sigma_0 A}{2}\left(b - \frac{\sigma_0 A}{0.85 a f_d}\right) \qquad (2)$$

Where a is the transversal edge length of the section, b the longitudinal length edge, A the section area, $\sigma_0 = W / A$ the average pre-compression (W: tower weight above the section considered) and f_d the design compressive strength. In what follows, obviously we assume $b = a = B$ and $A = B^2 - (B - 2t)^2$.

External moments, within a cantilever beam hypothesis (subdivided into n elements), may be evaluated at the generic section j as:

$$\begin{aligned} M_j &= F_{hj} z_j^* \\ z_j^* &= \frac{\sum_{i=1}^{j} z_i^2 W_i}{\sum_{i=1}^{n} z_i W_i} - z_j \\ F_{hj} &= \frac{\sum_{i=j}^{n} z_i W_i}{\sum_{i=1}^{n} z_i W_i} F_h \end{aligned} \qquad (3)$$

With $F_h = 0.85 S_d(T_1) W / g$ (S_d spectrum, T_1 first period of the structure, g gravity acceleration).

In order to evaluate the seismic vulnerability of the tower, the Italian code suggests the evaluation of the so-called acceleration factor $f_{a,SLV}$. The acceleration factor is the ratio between soil peak accelerations corresponding to the capacity and the expected demand:

$$f_{a,SLV} = \frac{a_{SLV}}{a_{g,SLV}} \qquad (4)$$

where a_{SLV} is the soil acceleration leading to the SLV ultimate state (SLV is an acronym that in the Italian Code indicates the ultimate limit state of life safeguard) and $a_{g,SLV}$ is the acceleration corresponding to the reference return period. The acceleration factor is a purely mechanical parameter, which may be useful for an evaluation of the weakness of the structure in terms of strength.

The evaluation of the acceleration of the response spectrum corresponding to the instant where SLV limit state is reached on the i-th section can be obtained taking into account the reduction induced by the confidence factor as follows:

$$S_{e,SLV,i}(T_1) = \frac{q g M_{R,i} \sum_{k=1}^{n} z_k W_k}{0.85 W F_C \left(\sum_{k=i}^{n} z_k^2 W_k - z_i \sum_{k=i}^{n} z_k W_k\right)} \qquad (5)$$

where q is the behavior factor, g the gravity acceleration, $M_{R,i}$ is the resistant bending moment on the i-th section, z_k and W_k are the height and the weight in correspondence of the k-th section, respectively, W the total weight, F_C the confidence factor (here assumed equal to 1.35), z_i the height of the i-th section with respect to the base and n the number of cross sections.

3.2 UDEC model

The distinct element method is an explicit method based on finite difference principles, derived from Cundall's original work (Cundall 1971). It is presented in the two dimensional code UDEC (Universal Distinct Element Code) and the three dimensional code 3DEC, developed for commercial use by Itasca Ltd for either the static or dynamic analysis (ITASCA 2004). UDEC was developed initially to model sliding rock masses in which failure occurs along the joints (Cundall 1971). This has similarities with the behaviour of low bond strength masonry which often encountered in masonry towers (Sarhosis et al. 2016a). Typical examples of masonry structures that have been modelled using the discrete element method and UDEC software include masonry arches (Sarhosis et al 2014; Forgacs et al. 2017); wall panels (Sarhosis et al. 2015; Sarhosis & Sheng 2014; Bui et al. 2017); and ancient colonnades (Sarhosis et al. 2016b; Pulatsu et al. 2017).

In UDEC, a masonry wall or a masonry structure can be represented as an assemblage of rigid or deformable distinct blocks which may take any arbitrary geometry. Rigid blocks do not change their geometry as a result of any applied loading and are mainly used when the behaviour of the system is dominated by the mortar joints. Deformable blocks are internally discretised into finite difference triangular zones and each element responds according to a prescribed linear or non-linear stress-strain law. Mortar joints are represented as zero thickness interfaces between the blocks. The soft contact approach is used, so a finite normal stiffness is taken to represent the measurable stiffness that exists at a contact or joint. A joint is represented numerically as a contact surface formed between two block edges. The representation of the interface between blocks relies on sets of point contacts (Sarhosis et al. 2016a). For each pair of blocks that touch (or are separated by a small gap), data elements are created to represent point contacts. Adjacent blocks can touch along a common edge segment or at discrete points where a corner meets an edge or another corner.

A point contact hypothesis is used, see Figure 3, i.e. where the interaction force at each contact is a function of solely the relative displacement between blocks at that location. When two blocks come into contact, a force develops between them which can be resolved into normal and shear components.

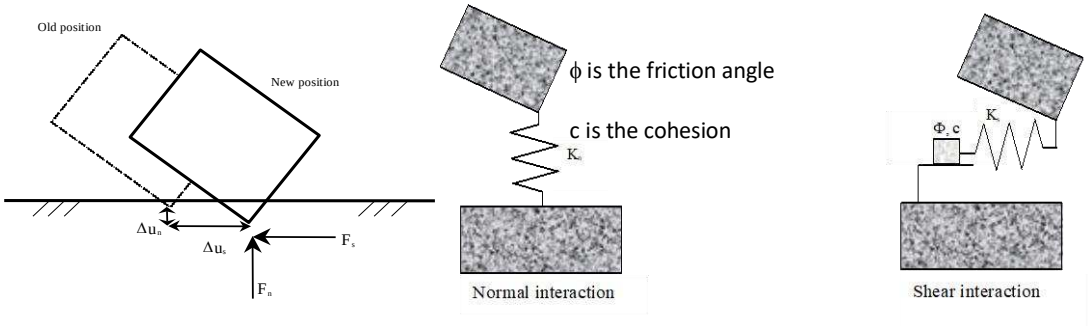

Figure 3. Forces between blocks (left) and Representation of joints (center and right) within DEM (blocks are in contact, separation is shown for clarity)

The simplest model of mechanical interaction is to assume that the blocks are connected by normal and shear elastic springs, Figure 3 (center and right), i.e. interaction forces are proportional to the relative displacement between the two blocks. This force-displacement law at the contacts is expressed in incremental form as:

$$\Delta F_n = K_n \Delta u_n$$
$$\Delta F_s = K_s \Delta u_s \qquad (6)$$

where ΔF_n and ΔF_n are the normal and shear force increments, Δu_n and Δu_s are the normal and shear displacement increments, K_n and K_s are the contact normal and shear stiffnesses.

Contacts between two block edges (Figure 4-a) can be represented by two corner-edge contacts. The contact length, l, allows contact stresses to be calculated as (assuming a unit thickness):

$$\sigma_n = F_n / l$$
$$\sigma_s = F_s / l \qquad (7)$$

and stress increments to be expressed in terms of the usual joint normal (k_n) and shear (k_s) stiffnesses (stress/length) as:

$$\Delta\sigma_n = k_n \Delta u_n$$
$$\Delta\sigma_s = k_s \Delta u_s \qquad (8)$$

When blocks are discretized into a fine internal mesh (deformable blocks), grid-points may be placed along the original edges (Figure 4-b). These grid-points are treated as new corners, since the edge is now able to deform into a polygonal line. The same expressions are used, with contact lengths defined as shown in Figure 4-b, and where the length associated with each grid-point is equal to half the distance between the two closest grid-points located to each side of the edge it contacts.

The overlaps displayed in these figures represent only a mathematically convenient way of measuring relative normal displacements. In finite element models, joints are similarly assigned a zero thickness, with overlapping indicating compressive joint stresses and separation indicating tension. If normal joint stiffness is increased, overlaps can be made as small as desired.

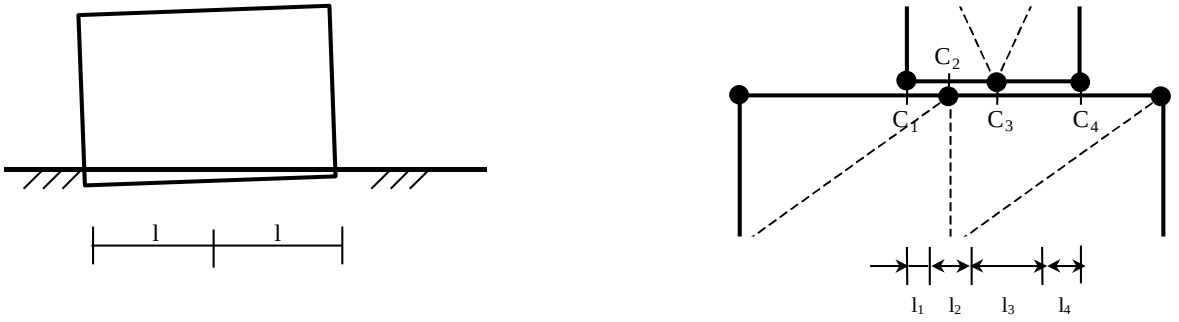

(a) Edge-edge contact

(b) Contact lengths for fully-deformable blocks

Figure 4. Contact between blocks.

A force-displacement law is used to find contact forces from known displacements. Incremental normal and shear displacements are calculated for each point contact.

The basic joint model is the Coulomb slip, see Figure 5, capable of capturing several of the features that are representative of the physical response of joints. The necessary parameters to be defined are the normal and shear stiffnesses (k_n and k_s), the friction angle (F) the cohesion (c) and the tensile strength (s_t).

For the joints simulating the characteristics of masonry, a Coulomb slip model (linear elastic with damage and residual strength) is sufficient in the majority of the cases, see Figure 5.

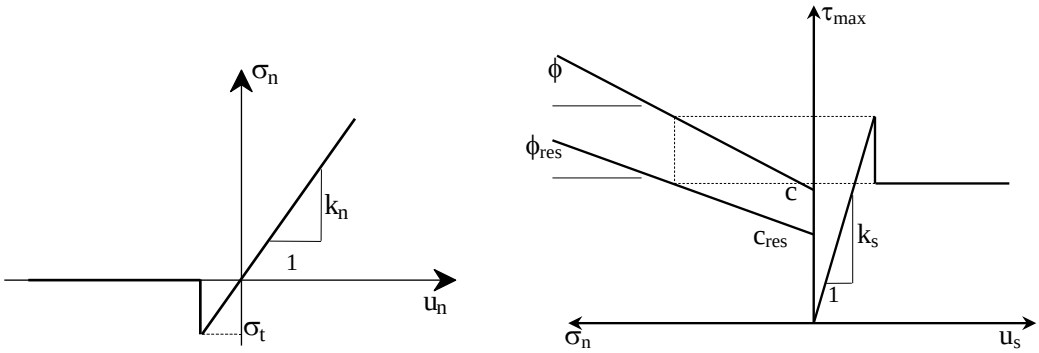

Figure 5: Interfaces between two blocks constitutive laws (normal and shear)

To perform pushover analyses, a so called "slow" dynamic approach is adopted, meaning that a distribution of horizontal forces is applied with a pre-assigned velocity and then the code finds the solution of the structural problem with an explicit approach, with possible non-linear behavior of the interfaces. This means that several dynamic analyses must be performed at different levels of the horizontal load applied to properly recover the entire global pushover curve. Obviously, before the application of any horizontal load, gravity loads are applied, as it occurs in common non-linear dynamic simulations.

Towers under consideration are discretized in UDEC as shown in Figure 1. Such discretization has the following characteristics:

1) It is two-dimensional, consistently with UDEC limitations, but takes into account the actual geometry assuming for the flanges (lateral walls) a thickness equal to B and for the core a thickness equal to 2t.
2) By means of the discretization adopted, the code can provide failure modes under a pure flexural behavior, pure shear, vertical cracks or a combination of the previous typical failure modes observed in practice.
3) It should be pointed out that the bottom row of elements in UDEC has been assigned as fixed in the horizontal and vertical direction, with potential consequences on the effective length of the towers in UDEC model. It is worth noting however that, when a no-tension material model is assumed and a failure due to the formation of a flexural hinge on the first horizontal interface from the ground, it is possible to find analytically the collapse load. If a reverse triangular distribution of horizontal actions is applied and 10 rows of elements are used (the most unfavorable mesh used here), it is easy to demonstrate that the ratio between the collapse load of the tower with interfaces at the base or shifted on the edge between first and second row of elements is 1.5/1.588, with a percentage error introduced equal to 5.87%, fully acceptable for practical purposes. In case of different failure modes, authors experienced that the error introduced is even lower. For this reason, it was made the choice to disregard this issue in the computations.

It is worth mentioning that mechanical properties to assume for the masonry material in UDEC should be the same used when dealing with Italian Guidelines method, see Table 2. There are quite precise indications provided by the Italian Code NTC2008 (2008), Chapter 8, and subsequent Explicative Notes in this regard. In the paper, values adopted for cohesion and masonry elastic moduli refer to a masonry typology constituted by clay bricks (approximate dimensions 210 x 52 x 100 mm^3) with very poor mechanical properties of the joint and quite regular courses. A low confidence factor $F_C = 1.35$ should be also assumed. Such kind of masonry is typical for towers located in the Northern Italy, but calculations can be repeated also assuming different mechanical characteristics according to the Italian Code. In the impossibility in UDEC to precisely assign all the inelastic parameters provided by the Italian code, for interfaces a pure Mohr-Coulomb behavior is assumed, with friction angle 30°, higher than that suggested by the Italian code, to compensate cohesion and tensile strength totally vanishing.

A typical series of pushover curves obtained with UDEC is depicted in Figure 6 (only D typology is shown for the sake of conciseness), whereas in Figure 7 and Figure 8 the failure mechanisms found at the end of the simulations for all the 16 towers are depicted. As can be appreciated, there are several different mechanisms active, depending on the geometry of the tower investigated, and ranging from a pure rocking at the base (e.g. A1, A3) to a vertical splitting into two parts (e.g. B3).

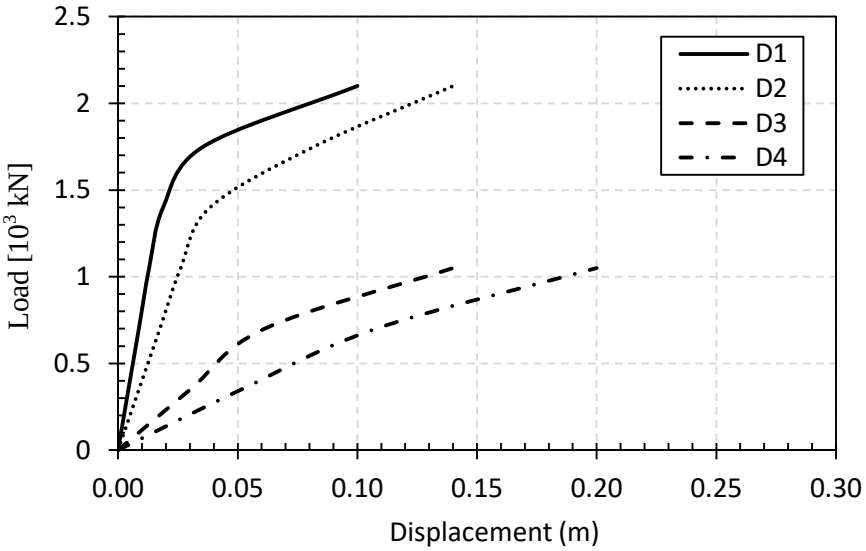

Figure 6: Typical pushover curves obtained with the software UDEC (D typology).

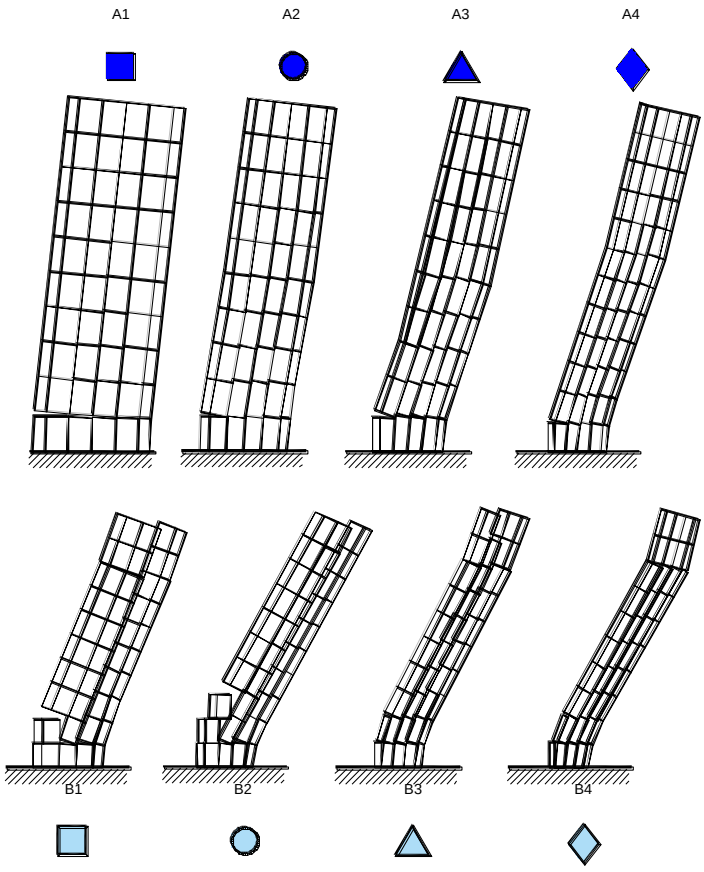

Figure 7: Failure mechanisms found with UDEC, towers A-B.

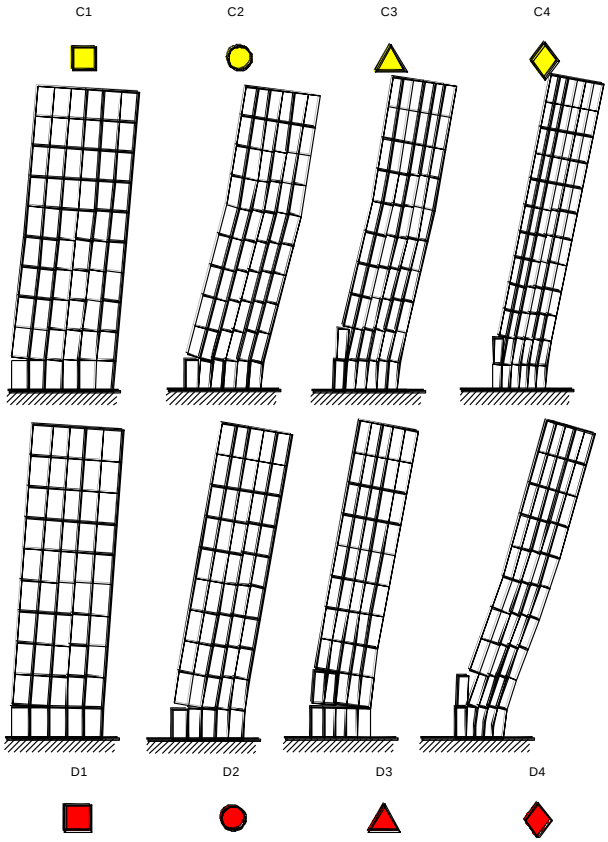

Figure 8: Failure mechanisms found with UDEC, towers C-D.

Table 2: Mechanical properties adopted for masonry and vaults infill

	f_m	τ_0	E	G	w
Masonry with clay bricks and poor mortar	MPa	MPa	MPa	MPa	kN/m^3
	2.4	0.06	1500	500	18

3.3 3Muri macro model

The four types (A, B, C and D) of towers under investigation have also been modelled by means of the 3Muri macro-elements analysis software (Galasco et al. 2002; Lagomarsino et al. 2013; Stadata 2016). Four masonry macro-elements have been assembled all together with effective joints at their intersection in order to create the box structure of the towers, which have been covered with a plane bi-directional rigid floor at the top (Figure 9-a). Therefore, towers are susceptible to undergo in-plane mechanisms only under the formation of shear and compression-bending failures, whereas local out-of-plane collapses have not been taken into account.

The same mechanical properties assumed for the previous two models have been adopted in 3Muri, see Table 2. A cracked condition has been assumed for Young and Shear moduli of the masonry, which however does not affect the calculation of the collapse acceleration. Linear dynamic (to estimate the first vibration mode) and non-linear static analyses have been performed on the towers considered.

It is worth noting that, in practice, the evaluation of the ultimate load can be also carried out with manual calculations on the two shear walls loaded in plane, following Italian code formulas.

Recalling the general Italian code NTC 2008, resisting shear V_t and bending moment for a masonry wall should be evaluated as follows. V_t assumes for existing buildings the following value (for diagonal cracks or Turnsek and Cacovic formula):

$$V_t = Lt \frac{1.5\tau_{0d}}{b} \sqrt{1 + \frac{\sigma_0}{1.5\tau_{0d}}} \qquad (9)$$

where:

- $L = B - t$ and t are the panel width and thickness respectively;
- b is a coefficient depending on the panel slenderness. For $H/b > 1.5$ it should be , but it is worth noting that the coefficient b is applicable in the case of a perforated wall modelled by the equivalent frame approach; in the case of a tower, each panel represents the web of the hollow section, where shear stresses are almost constant. Therefore, b=1 is used.
- τ_{0d} is masonry reference shear strength, obtained from the average masonry shear strength τ_0 by means of the relation $\tau_{0d} = \tau_0 / F_c$, with F_C already defined;
- σ_0 is the average vertical compressive stress, defined as $\sigma_0 = N / Lt$, where N is the normal action on the panel at the iteration considered.

On the other hand, V_t is evaluated for new structures as follows (base sliding shear):

$$V_t = L'tf_{vd} \qquad (10)$$

Where:

- L' is the width of the compressed zone;
- $f_{vd} = (\tau_0 + 0.4\sigma_n)/F_c$ is the design masonry shear strength. Here σ_n is the average compressive stress action on L' (i.e. $\sigma_n = N / L't$). The numerical coefficient 0.4 in the formula plays the role of friction, being the value of f_{vd} clearly obtained by means of the Mohr-Coulomb formula.

In the majority of the cases, Eq. (4) furnishes values of V_t greater than Eq. (5) and this is the reason why here Eq. (5) is used.

Finally, ultimate bending moment for rocking failure can be evaluated as follows:

$$M_u = (L^2 t\sigma_0 / 2)(1 - \sigma_0 / 0.85 f_d) \qquad (11)$$

Where $f_d = f_m / F_c$, with f_m masonry average compressive strength ($f_m = f_k / 0.7$, f_k characteristic value). It is interesting to notice that Eq. (11) is conceptually identical to Eq. (2) and this is not surprising because the theoretical base is the same.

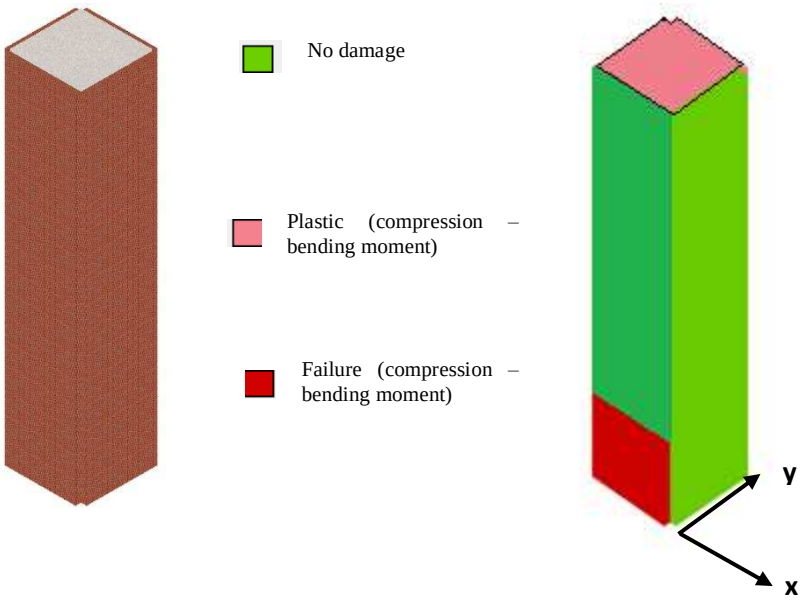

-a -b

Figure 9: Seismic pushover analysis in direction x with accidental eccentricity: the 3Muri model (a) and (-b) collapse mechanism experienced for all towers.

The collapse mechanisms found with the pushover analyses conducted with 3Muri showed always rocking failure (Figure 9-b). It is interesting to notice that when a seismic accidental eccentricity is

considered, in all cases towers with the lowest slenderness (A1, B1, C1 and D1) exhibit the strongest coupling between translational displacement and torsion rotation, whereas all the remaining towers have a less pronounced torsion. However, it is worth noting that in the evaluation of the collapse acceleration to compare with other approaches, accidental eccentric is not taken into account, in order not to introduce possible causes of deviation from the expected results, being such parameter not considered in other approaches. It is also correct to disregard accidental eccentricity, not only because UDEC 2D model and the simplified formulation do not consider it, but because in this kind of structures the accidental loads are negligible, in comparison with permanent ones. In all investigated cases, towers show compression-bending plastic behavior and collapses only, without exhibiting shear failures. This is confirmed by the manual application of formula (11) on the two walls parallel to the application of the seismic load. Since Eq. (11) is theoretically identical to Eq. (2), but the former is applied only on two walls with thickness t_1 and not on a hollow section, it is expected that 3Muri furnishes a much smaller collapse acceleration, as confirmed by the results shown in the following Section.

4 Straightforward interpolation formulas

Results obtained with the three models proposed in terms of normalized collapse acceleration are depicted from Figure 10 to Figure 12. In particular, Figure 10 refers to Italian Guidelines, Figure 11 to UDEC and Figure 12 to 3Muri. In the horizontal axis, slenderness is represented.

A fitting exponential function is also reported with the corresponding equation, in order to give the possibility to any practitioner interested to enter into the diagrams and predict an acceleration at collapse on a real tower without the need to perform any computation. As a matter of fact, only the value of slenderness is needed.

From an overall analysis of the obtained results, the following considerations are worth noting:

1) Italian Guidelines and 3Muri outputs are almost completely independent from the normalized cross shear area, as shown by Figure 10 and Figure 12, where blue symbols almost superimpose with the corresponding red ones. Such results are quite obvious, because the observed failure mechanisms in 3Muri are flexural and the Italian Guidelines a priori exclude shear failures. In addition, as far as the Italian Guidelines are concerned, the evaluation of the resistant bending moment by means of formula (2) is little influenced by walls thickness, and this explains the small differences observed between series D (large shear area) and A (small shear area).
2) UDEC results are quite sensible to shear area (see Figure 11), especially and as expected for low slenderness, i.e. where a shear failure is more likely. When slenderness increases, the two fitting curves (one for large shear areas the other for small shear areas) tend obviously to coincide, a clear indication that failure is purely flexural.
3) Fitting function provided by 3Muri stands on the safe size, because the load carrying capacity (as already discussed) is evaluated only considering the two shear walls parallel to the horizontal action, whereas the actual hollow cross section should be considered to properly account for the box behavior favored by transversal walls. The most realistic prediction is provided by UDEC analyses, which are also sensitive to the different shear areas of the towers, thus providing, albeit approximate, an implicit indication on the failure mode.

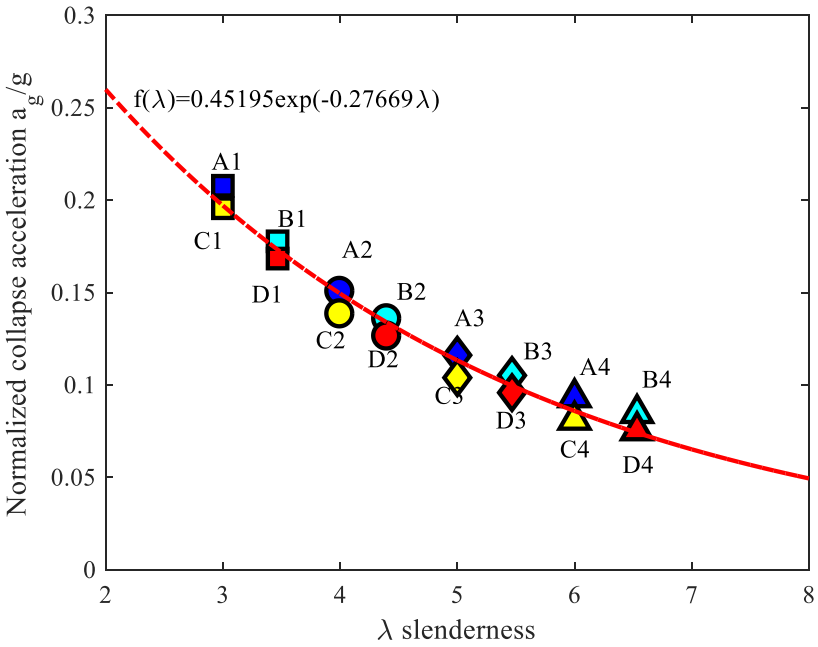

Figure 10: Italian Guidelines for the Built Heritage. Normalized collapse acceleration a_g/g vs slenderness and corresponding exponential fitting function.

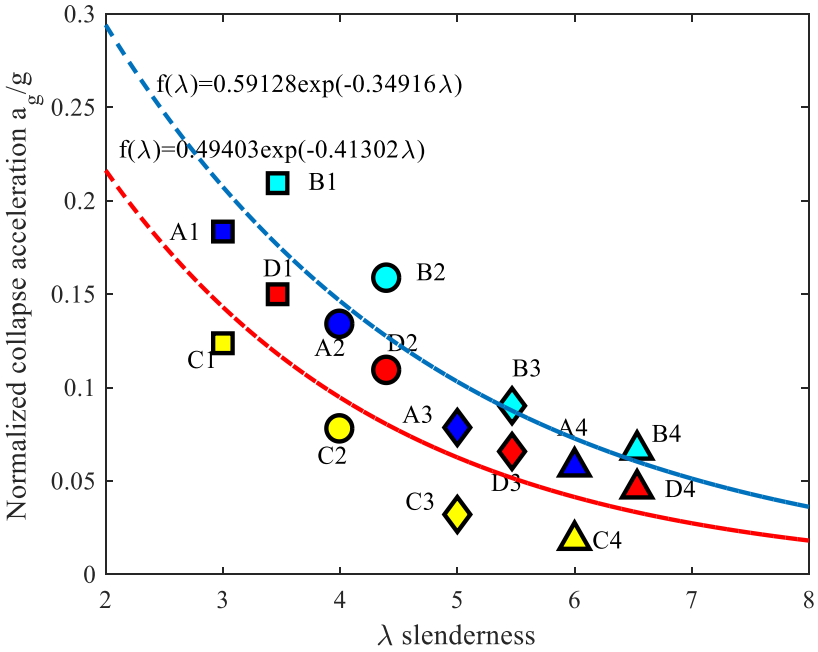

Figure 11: UDEC software. Normalized collapse acceleration a_g/g vs slenderness and corresponding exponential fitting function.

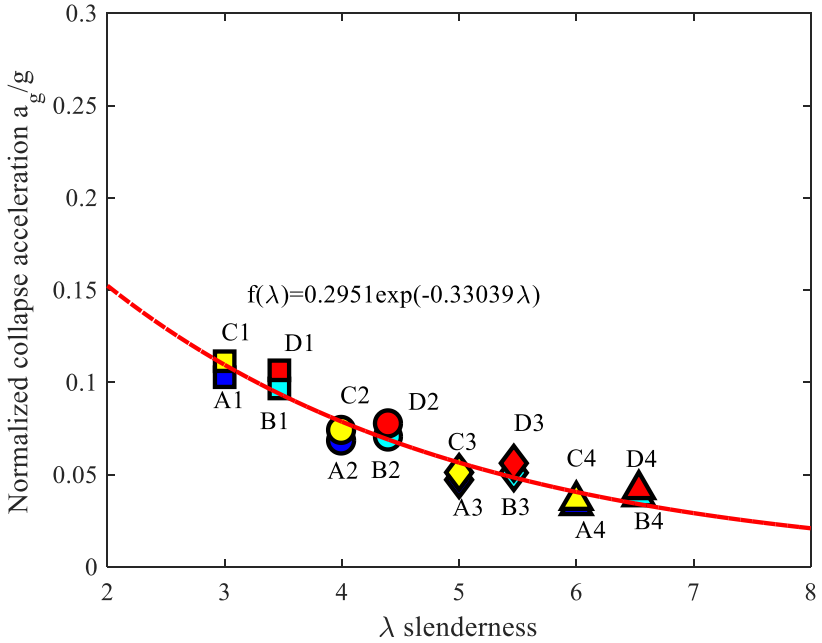

Figure 12: 3Muri software. Normalized collapse acceleration a_g/g vs slenderness and corresponding exponential fitting function.

5 Limit analysis with pre-assigned failure mechanisms

Sampling a limited number of pre-assigned failure mechanisms deduced from past earthquake experiences, it is possible to apply repeatedly the principle of virtual powers (in the framework of the upper bound theorem of limit analysis) and estimate very quickly a possible collapse acceleration a_g normalized against the gravity acceleration g (it can be easily shown that a_g/g corresponds to the collapse load) exhibited by a certain ideal tower, univocally defined by the knowledge of its height H, base B and wall thicknesses t_1.

In this framework, large scale Monte Carlo MC simulations can be repeated on such "ideal" towers (i.e. with square cross section and constant thickness) at a fraction of the effort needed in standard FE computations.

For the sake of simplicity, we limited the study to few probable collapse mechanisms, assuming that the ideal tower can fail according to the five different schemes depicted in Figure 13. The choice is of course arbitrary but is based on the phenomenological awareness that they are the most probable, at least in practice.

Mechanism #1 is typically observed for many existing masonry towers and is constituted by the vertical splitting into two portions and the rocking of such portions near the base. It is worth mentioning here that vertical ultimate shear τ_{v0} (i.e. shear stress along a vertical crack) should be higher than the horizontal one τ_{h0} (because of the interlocking effect, at least for regular masonry textures). However, to distinguish between τ_{v0} and τ_{h0} would require the introduction of a further geometric parameter influencing load carrying capacities, namely masonry texture. As a matter of fact, different textures (considering also quasi periodic and random patterns) result into completely different orthotropic parameters for the masonry behavior at failure, as shown for instance in Milani et al. (2006a). The present paper is however devoted exclusively to the analysis of the behavior of towers as a consequence of their geometric features. Authors believe that, due to the variety and complexity of the patterns that can be encountered in practice, such analysis deserves dedicated research that is postponed in a specialized research.

Mechanism #2 is a monolithic rocking of the tower with cylindrical hinge at the base; such mechanism is the closest to Italian Code one.
Mechanisms #3 exhibits an inclined crack pattern departing from the base, with consequent rocking of the upper part around the cylindrical hinge located on the compressed toe. It has been demonstrated by Heyman (1995) that such mechanism activates in case of leaning towers with full cross section and under the hypothesis of no tension material for masonry.
Mechanism #4 is a combination of Heyman's rocking and vertical splitting. It is worth noting that the sliding of the left block guarantees plastic admissibility on interfaces under the failure criterion adopted in the analyses.
Finally, Mechanism #5 is a sliding of the upper part on a horizontal interface located near the base.
It is worth noting that all mechanisms are admissible from a kinematic limit analysis standpoint. As a matter of fact, assuming for masonry the multi-surface isotropic failure criterion shown in Figure 14-a, the jumps of displacements sketched in Figure 13 turn out to obey the plastic flow admissibility. It is interesting to notice that, for the sake of simplicity, we assumed a decoupled behavior between tangential and normal stresses. A more rigorous approach would require the adoption of a Mohr-Coulomb failure criterion, which however is characterized by a slight complication in the definition of the jump of velocities on interfaces, since in this latter case a tangential velocity on an interface is always associated to a normal component.
Such failure surface, which is obviously simplified, is consistent with the manual mechanisms of Figure 13 in terms of respect of the plasticity associated flow rule. In Mechanism #1, for instance, in case of adoption of classic limit analysis with a Mohr-Coulomb failure criterion, there would be axial separation between the right and left parts along the vertical crack, which is not present with the simplified approach proposed. The aim is to simplify computations to a great extent, in order to provide closed form formulas to give to practitioners and that can be used in common electronic spreadsheets. This, however, does not mean that the typical cohesive frictional behavior of masonry is lost, because the effect of the normal stress on tangential strength is taken into account increasing the ultimate shear strength according to the classic Mohr-Coulomb law. The typical increase of shear strength due to gravity loads (and friction angle) is taken indeed into account in Mechanism #5 when computing internal dissipation for horizontal cracks subjected to sliding, see Figure 13.Vertical stress acting on cracks is assumed equal to self-weight over the cross area, again a simplification commonly accepted in the specialized literature. On the other hand, authors experienced that the error committed in the evaluation of the collapse load for Mechanism #1 is lower than 1%, when as reference is assumed the rigorous associated plasticity approach. Similar outcomes are obtained for the other mechanisms.
Large scale Monte Carlo simulations ($5x10^6$ of samples) are performed changing in a wide range tower height H, slenderness λ and normalized shear area ξ. It is worth noting that the knowledge of H, λ and ξ allows immediately evaluating the base width B and wall thicknesses t_1 as follows:

$$\begin{aligned} B &= \lambda H \\ t_1 &= B\left(1-\sqrt{\xi}\right) \end{aligned} \qquad (12)$$

In order to cover a wide range of possibilities that can be encountered in practical design, we adopted the following ranges for the geometric variability of the parameters: H between 5 and 80 m, λ between 1.5 and 15 and ξ between 0.1 and 0.9.

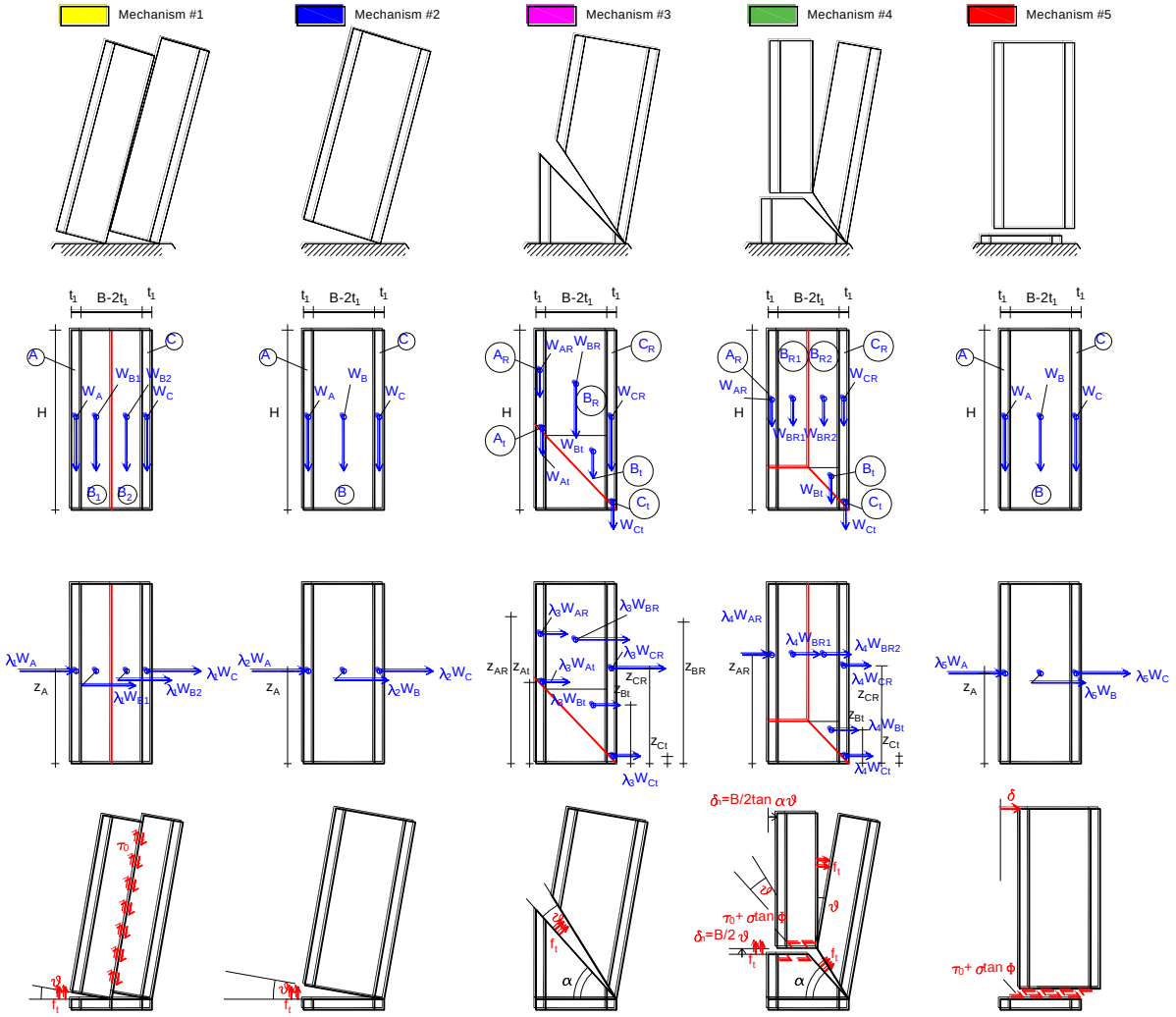

Figure 13: Different mechanisms considered in the kinematic simplified limit analysis approach proposed. Mechanism #1, rocking with vertical splitting. Mechanism #2, monolithic rocking. Mechanims #3, Heyman's diagonal cracking and rocking. Mechanism #4, mixed Heyman's mechanism with vertical splitting. Mechanism #5, base shear sliding.

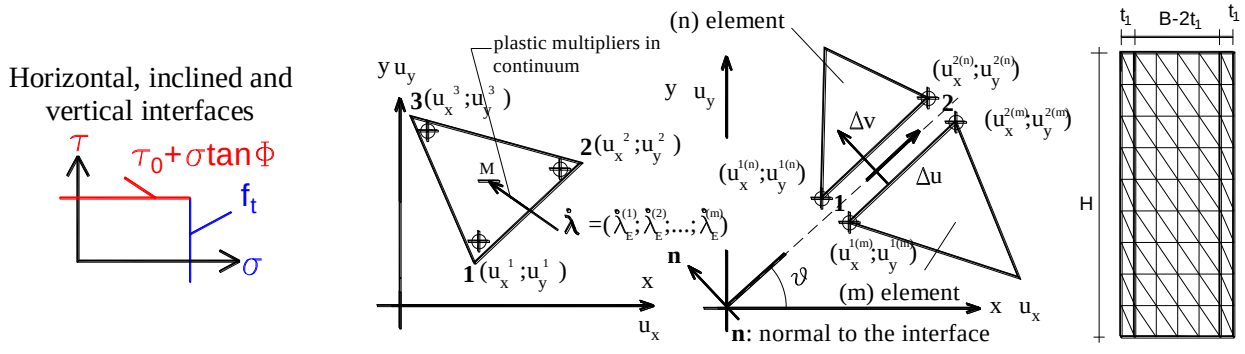

(a) (b)

Figure 14 (a) simplified failure surface adopted for the interfaces in Figure 13; (b) Triangular element used in the upper bound FE limit analysis (left), velocity jumps on interfaces between adjacent triangles (middle) and parametric FE mesh used to perform MC simulations with the kinematic FE limit analysis (right).

- **Mechanism #1**

Mechanism 1 is a combination of rocking around the base with vertical splitting into two parts. It is worth mentioning that such mechanism is frequently observed during post-earthquake surveys on collapsed towers.

According to the sketch shown in Figure 13, the collapse multiplier associated to such mechanism is the following:

$$\lambda_1 = \frac{W_A\frac{B-t_1}{2} + W_{B_1}\left(\frac{B}{4}-\frac{t_1}{2}\right) + W_{B_2}\left(\frac{B}{4}-\frac{t_1}{2}\right) + W_C\frac{t_1}{2} + \tau_0 BHt_2 + f_t a t_1\frac{B-t_1}{2} + f_t t_2\left(\frac{B}{2}-t_1\right)^2 + f_t t_2\left(\frac{B}{2}+t_1\right)\left(\frac{B}{2}-t_1\right) + f_t a t_1\frac{t_1}{2}}{z_A\left(W_A + W_{B_1} + W_{B_2} + W_C\right)} \quad (13)$$

Where, exception made for symbols already introduced, the different quantities (see also Figure 13) can be evaluated as follows:

- $W_A = t_1 a H \gamma_M$, $W_{B_1} = t_2 B H \gamma_M$, $W_{B_2} = t_2 B H \gamma_M$ and $W_C = t_1 a H \gamma_M$ are the different weight of the blocks (γ_M is masonry specific weight);
- a is tower width along the transversal direction and here kept equal to B and t_2 is the thickness of the walls along the longitudinal direction;
- z_A is the vertical position of the horizontal load dependent on the load multiplier, which in this case it is kept equal to $z_A = \frac{H}{2}$ in agreement with classic limit analysis computations, even if Italian Code utilizes a reverse triangular distribution of seismic loads, i.e. $z_A = \frac{2H}{3}$. However, it is worth mentioning that no theoretical difficulties arise if a triangular distribution assumed instead of the classic constant one.

- **Mechanism #2**

According again to Figure 13, Mechanism #2 is a simple rocking around the base, which is the mechanism closest to the Italian code. Some differences are however noticeable, as for instance the different evaluation of the ultimate bending moment for the Italian code, which involves a cantilever beam approach, a limited compressive strength and a simplified evaluation for hollow sections. These results in a different evaluation of the collapse acceleration, as will be shown later on. The collapse multiplier associated to Mechanism #2 is the following:

$$\lambda_2 = \frac{W_A\left(B-\frac{t_1}{2}\right) + W_B\frac{B}{2} + W_C\frac{t_1}{2} + f_t a t_2\left(B-\frac{t_1}{2}\right) + f_t 2t_2\left(B-2t_1\right)\frac{B}{2} + f_t a t_2\frac{t_1}{2}}{z_A\left(W_A + W_B + W_C\right)} \quad (14)$$

Where $W_B = W_{B1} + W_{B2}$, $z_A = \frac{H}{2}$ and all the other symbols have been already introduced.

- **Mechanism #3**

With reference to Figure 13 , Mechanism #3 inspired by the results found by Heyman **Ref** in case of leaning towers. The analogy between leaning towers and seismic load makes sense because it can be easily shown, indeed, that the out-of-verticality angle has the same effect of the application of a horizontal load. Assuming masonry unable to withstand tensile stresses, Heyman shown that a limit out-of-verticality exists that makes the tower collapse under gravity loads for the formation of a mechanism constituted by a diagonal crack departing from the base and ending on the opposite side, having a non-linear shape. Heyman discussed his results for a full rectangular cross section. It can be easily shown that the linearization of the crack curve forming the mechanism is affected by an error of about 3% on the collapse load, therefore fully acceptable for practical purposes. The procedure of linearization can be repeated for a hollow thin walled cross section. It can be proved that the angle α in Figure 13 assumes the following values: $\tan\alpha = 0.573H/B$ and $\tan\alpha = 0.20H/B$ for full and hollow thin walled sections, respectively. In the Monte Carlo simulations treated hereafter we use a linear interpolation between the two values in order to take approximately into account the real thickness of the walls.

Under such hypotheses, the collapse multiplier is the following:

$$\lambda_3 = \frac{W_{AR}x_{AR} + W_{At}x_{At} + W_{BR}x_{BR} + W_{Bt}x_{Bt} + W_{CR}x_{CR} + W_{Ct}x_{Ct} + P_i}{W_{AR}z_{AR} + W_{At}z_{At} + W_{BR}z_{BR} + W_{Bt}z_{Bt} + W_{CR}z_{CR} + W_{Ct}z_{Ct}} \qquad (15)$$

Where the symbols have the following meaning:

- $W_{AR} = at_1(H - B\tan\alpha)\gamma_M \quad z_{AR} = B\tan\alpha + \frac{H}{2} - \frac{B}{2}\tan\alpha \quad x_{AR} = B - \frac{t_1}{2}$;
- $W_{At} = \frac{1}{2}at_1^2\tan\alpha\gamma_M \quad z_{At} = B\tan\alpha - \frac{1}{3}t_1\tan\alpha \quad x_{At} = B - \frac{2}{3}t_1$;
- $W_{BR} = (B-2t_1)2t_2\left[H - (B-t_1)\tan\alpha\right]\gamma_M \quad z_{BR} = H - \frac{1}{2}\left[H - (B-t_1)\tan\alpha\right] \quad x_{BR} = \frac{B}{2}$;
- $W_{Bt} = \frac{1}{2}(B-2t_1)2t_2\left[(B-2t_1)\tan\alpha\right]\gamma_M \quad z_{Bt} = t_1\tan\alpha + \frac{2}{3}\left[(B-2t_1)\tan\alpha\right] \quad x_{Bt} = t_1 + \frac{1}{3}(B-2t_1)$;
- $W_{CR} = (H - t_1\tan\alpha)t_1a\gamma_M \quad z_{CR} = t_1\tan\alpha + \frac{1}{2}\left[H - t_1\tan\alpha\right] \quad x_{CR} = \frac{t_1}{2}$;
- $W_{Ct} = \frac{1}{2}t_1^2\tan\alpha\gamma_M \quad z_{Ct} = \frac{2}{3}t_1\tan\alpha \quad x_{Ct} = \frac{t_1}{3}$;
- $P_i = \frac{1}{2}Bf_t\left(\frac{t_1}{\cos\alpha}\right)^2 + t_2 f_t\left[\left(\frac{B-t_1}{\cos\alpha}\right)^2 - \left(\frac{t_1}{\cos\alpha}\right)^2\right] + \frac{1}{2}Bf_t\left[\left(\frac{B}{\cos\alpha}\right)^2 - \left(\frac{B-t_1}{\cos\alpha}\right)^2\right]$.

- **Mechanism #4**

Mechanism #4, Figure 13, is a combination between Heyman's failure mechanism and vertical splitting in the middle section. It is sometimes observed in real cases and also is provided by UDEC code, compare for instance Figure 7 and Figure 8.

Assuming such composite mechanism, the collapse load can be evaluated using the following formula:

$$\lambda_4 = \frac{W_{AR}x_{AR} + W_{B1R}x_{B1R} + W_{B2R}x_{B2R} + W_{B2t}x_{B2t} + W_{CR}x_{CR} + W_{Ct}x_{Ct} + P_i}{W_{AR}z_{AR} + W_{B1R}z_{B1R} + W_{B2R}z_{B2R} + W_{B2t}z_{B2t} + W_{CR}z_{CR} + W_{Ct}z_{Ct}} \qquad (16)$$

Where the symbols have the following meaning:

- $W_{AR} = \left(H - \frac{B}{2}\tan\alpha\right)at_1\gamma_M \quad z_{AR} = \frac{1}{2}\left(H - \frac{B}{2}\tan\alpha\right) \quad x_{AR} = \frac{B}{2} - \frac{t_1}{2}$;
- $W_{B1R} = \left(\frac{B}{2} - t_1\right)2t_2\left(H - \frac{B}{2}\tan\alpha\right)\gamma_M \quad z_{B1R} = \frac{1}{2}\left(H - \frac{B}{2}\tan\alpha\right) \quad x_{B1R} = \frac{1}{2}\left(\frac{B}{2} - t_1\right)$;
- $W_{B2R} = \left(\frac{B}{2} - t_1\right)2t_2\left(H - \frac{B}{2}\tan\alpha\right)\gamma_M \quad z_{B2R} = \frac{B}{2}\tan\alpha + \frac{1}{2}\left(H - \frac{B}{2}\tan\alpha\right) \quad x_{B2R} = t_1 + \frac{1}{2}\left(\frac{B}{2} - t_1\right)$
- $W_{B2t} = \frac{1}{2}\frac{B}{2}\tan\alpha\left(\frac{B}{2} - t_1\right)2t_2\gamma_M \quad z_{B2t} = \frac{2}{3}\frac{B}{2}\tan\alpha \quad x_{B2t} = t_1 + \frac{1}{3}\left(\frac{B}{2} - t_1\right)$;
- $W_{CR} = (H - t_1\tan\alpha)t_1a\gamma_M \quad z_{CR} = t_1\tan\alpha + \frac{1}{2}(H - t_1\tan\alpha) \quad x_{CR} = \frac{t_1}{2}$;
- $W_{Ct} = \frac{1}{2}t_1^2\tan\alpha\gamma_M \quad z_{Ct} = \frac{2}{3}t_1\tan\alpha \quad x_{Ct} = \frac{t_1}{3}$;
- $P_i = \frac{1}{2}af_t\left(\frac{t_1}{\cos\alpha}\right)^2 + 2t_2 f_t\left(\frac{\frac{B}{2} - t_1}{\cos\alpha}\right)\left(\frac{\frac{B}{4} + \frac{t_1}{2}}{\cos\alpha}\right) + f_t t_2\left(H - \frac{B}{2}\tan\alpha\right)^2 + \tau_0\left[at_1 + 2t_2\left(\frac{B}{2} - t_1\right)\right]\frac{B}{2}\tan\alpha$.

- **Mechanism #5**

The last Mechanism #5, Figure 13, is a pure shear sliding at the base, which is expected to be possible for small slenderness and low friction angles.

The associated collapse multiplier is the following:

$$\lambda_5 = \frac{\tau\left[2at_1 + 2t_2(B - 2t_1)\right]}{W_A + W_B + W_C} \qquad (17)$$

Where we assume that $\tau = \tau_0 + \frac{W_A + W_B + W_C}{aB - (a - 2t_2)(B - 2t_1)} \tan\Phi$. It is worth noting that the simplified failure surface adopted in the computations, see Figure 14, allows for an independent deformation of the interface under shear and normal actions. This implies that blocks are not subjected to a spurious displacement due to the fulfilment of plastic admissibility on the interfaces, but at the same time the Mohr-Coulomb behavior (i.e. increase of the tensile strength with pre-compression, ruled by the friction angle) is preserved.
In the framework of the upper bound theorem of limit analysis, the failure mechanism active is associated to the minimum of the collapse loads evaluated from Eq. (13) to (17), which represents the a_g/g ratio that the tower can carry in an incipient state of failure.

6 Limit analysis with an upper bound triangular FE approach

MC simulations can be also performed with a 2D FE kinematic limit analysis software, as that proposed by one of the authors in Milani et al. (2006b).
Such FE limit analysis approach is based on the upper bound theorem of limit analysis and uses triangular elements with linear interpolation of the velocity fields and interfaces, Figure 14-b, where velocity jumps can occur. Classically, to find the collapse load of a structure with a finite element discretization, in the framework of the upper bound theorem, a linear programming problem is written where the objective function to minimize (under equality and inequality constraints) is represented by the total internal power dissipated.
Equality constraints collect compatibility, plastic flow in continuum and on interfaces and boundary conditions.
For the sake of clarification, hereafter we discuss in brief some of the most important features on the constraints to be imposed, referring the reader to Milani et al. (2006b) for further details. As a matter of fact, one important equality set of constraints to be imposed at the interface between two adjoining elements $(m)-(n)$, involves nodal velocities of the elements and jumps of velocity on the common interface. In particular, it can be easily shown that after trivial algebra, the tangential and normal jumps on interfaces depend linearly on the Cartesian nodal velocities of elements $(m)-(n)$, resulting into four linear equalities per interface, that in a general form are written as $\mathbf{A}_{11}^{eq}\mathbf{u}^{Em} + \mathbf{A}_{12}^{eq}\mathbf{u}^{En} + \mathbf{A}_{13}^{eq}\Delta\mathbf{u} = \mathbf{0}$, where $\Delta\mathbf{u}$ is a $4x1$ vector collecting velocity jumps of the interface nodes (one tangential and one normal per node), $\mathbf{u}^{Em}$ and $\mathbf{u}^{En}$ are the $6x1$ vectors collecting the velocities of the elements (m) and (n) respectively, $\mathbf{A}_{11}^{eq}$ and $\mathbf{A}_{12}^{eq}$ are $4x9$ matrices depending only on nodal coordinates of element (m) and (n), respectively, and $\mathbf{A}_{13}^{eq}$ is a $4x4$ geometric matrix of the interface.
Another important set of equality constraints representing the plastic flow in continuum (obeying an associated flow rule) must be written for each triangular element. In particular, three equations must be written as follows:

$$\dot{\boldsymbol{\varepsilon}}_{pl}^{E} = \left[\frac{\partial u_x}{\partial x} \quad \frac{\partial u_y}{\partial y} \quad \frac{\partial u_y}{\partial x} + \frac{\partial u_x}{\partial y}\right] = \dot{\lambda}^{E} \frac{\partial S^{C}}{\partial \boldsymbol{\Sigma}^{C}} \qquad (18)$$

where $\dot{\boldsymbol{\varepsilon}}_{pl}^{E}$ is the plastic strain rate vector of element E, $\dot{\lambda}^{E} \geq 0$ is the plastic multiplier, S^{C} indicates a generic (non) linear failure surface for continuum and $\boldsymbol{\Sigma}^{C} = \left[\sigma_x \quad \sigma_y \quad \tau\right]^{T}$ is the plane-stress vector in continuum (σ_x: normal x-axis stress, σ_y: normal y-axis stress, τ: tangential stress).
There is the possibility to solve the limit analysis problem using consolidated linear programming routines, after a suitable linearization with m planes of the failure surface in the form $S^{C} \equiv \mathbf{A}^{in}\boldsymbol{\Sigma}^{C} \leq \mathbf{b}^{in}$, where $\mathbf{A}^{in}$ is a $mx3$ matrix (each row corresponds to coefficients of one

linearization plane) and $\mathbf{b}^{in}$ is the mx1 vector of linearization planes right hand sides. Within such assumption, and remembering that the velocity interpolation inside one triangular element is linear, three linear equality constraints per element can be written as $\mathbf{A}_{21}^{eq}\mathbf{u}^{E} + \left(\mathbf{A}^{in}\right)^{T}\dot{\boldsymbol{\lambda}}^{E} = \mathbf{0}$ where $\mathbf{u}^{E}$ is the vector of element velocities, $\dot{\boldsymbol{\lambda}}^{E}$ is the mx1 vector of plastic multiplier rates of the element (one for each plane of the failure surface), and $\mathbf{A}_{21}^{eq}$ is a 3x6 matrix of coefficients depending on the coordinates of the element nodes.

It is worth also noting that, analogously to continuum, a similar set of equality constraints must be imposed for interfaces in order to cope with the plastic flow condition on interfaces.

Boundary conditions translate into mathematics with further equality constraints, whereas the admissibility of the plastic flow requires that plastic multiplier rates (of interfaces and continuum) are non-negative, being strictly positive only those active, i.e. associated to a plasticization of the node.

After some elementary assemblage operations, a simple linear programming problem is obtained (the reader is again referred to Milani et al. (2006b) for a comprehensive discussion on the topic) where the objective function is represented by the total internal power dissipated minus the power expended by the loads independent from the load multiplier:

$$\begin{cases} \min\left\{\left(\mathbf{b}_{ass}^{in}\right)^{T}\dot{\boldsymbol{\lambda}}_{E}^{ass} + \left(\mathbf{b}_{I,ass}^{in}\right)^{T}\dot{\boldsymbol{\lambda}}_{I}^{ass} - \mathbf{P}_{0}^{T}\mathbf{u}\right\} \\ \text{such that}\begin{cases} \mathbf{A}^{eq}\mathbf{U} = \mathbf{b}^{eq} \\ \dot{\boldsymbol{\lambda}}_{E}^{ass} \geq \mathbf{0} \\ \dot{\boldsymbol{\lambda}}_{I}^{ass} \geq \mathbf{0} \end{cases} \end{cases} \qquad (19)$$

where:

- $\mathbf{b}_{ass}^{in}$ and $\mathbf{b}_{I,ass}^{in}$ are the assembled right-hand sides of the inequalities, which determine the linearised failure surface of the material of the continuum and of the interfaces, respectively;
- $\mathbf{P}_0$ is the vector of nodal loads independent from the load multiplier;
- $\mathbf{U} = \left[\mathbf{u}^{T} \quad \left(\dot{\boldsymbol{\lambda}}_{E}^{ass}\right)^{T} \quad \left(\Delta\mathbf{u}^{ass}\right)^{T} \quad \left(\dot{\boldsymbol{\lambda}}_{I}^{ass}\right)^{T}\right]^{T}$ is the vector of global variables, which collects the vector of assembled nodal velocities ($\mathbf{u}$), the vector of assembled element plastic multiplier rates ($\dot{\boldsymbol{\lambda}}_{E}^{ass}$), the vector of assembled velocity jumps on interfaces ($\Delta\mathbf{u}^{ass}$), and the vector of assembled interface plastic multiplier rates ($\dot{\boldsymbol{\lambda}}_{I}^{ass}$);
- $\mathbf{A}^{eq}$ is the overall constraints matrix and collects velocity boundary conditions, relations between velocity jumps on interfaces and elements velocities, constraints for plastic flow in velocity discontinuities and constraints for plastic flow in continuum.

It is worth noting that $\left(\mathbf{b}_{ass}^{in}\right)^{T}\dot{\boldsymbol{\lambda}}_{E}^{ass}$ and $\left(\mathbf{b}_{I,ass}^{in}\right)^{T}\dot{\boldsymbol{\lambda}}_{I}^{ass}$ in the objective function represents the total power dissipated by the continuum and by the interfaces, respectively.

Within a computations scheme where MC simulations must be performed, we assume the parametric mesh shown in Figure 14-b, which is sufficiently flexible to allow to speed up limit analysis computations, without the need to utilize a new mesh for the following simulation.

A total of 100000 FE simulations have been performed, which took more than 5 days of processing time on a common PC with 8Gb RAM. Whilst limit analysis with pre-assigned failure mechanisms allow for larger simulations (hereafter a $5x10^{6}$ cloud of points is utilized) with a minimal computational effort (less than 2 minutes), FE limit analysis can be regarded as a further validation of the approach proposed, because at least theoretically a procedure based on pre-assigned failure

mechanisms could in principle overestimate collapse loads, with an incorrect evaluation of the active failure mechanism.

7 Results of MC simulations

Monte Carlo simulations are conducted on a population of $5x10^6$ ideal towers utilizing the approach based on the five pre-assigned failure mechanisms.
Three sets of simulations are repeated, changing slightly the mechanical properties of the interfaces according to the sensitivity scheme summarized in Table 3.
From a detailed analysis of Table 3, it can be observed that Case 1 is characterized by a fairly good cohesion for the interfaces, an almost vanishing tensile strength (which well approximates the no-tension material hypothesis done by both the Italian Code and Heyman 1995) and a reasonable friction angle, very near to that assumed by Italian Code NTC 2008. Case 2 is characterized by vanishing cohesion and tensile strength and small friction angle. This situation, as it will be discussed later on, favors a sliding failure mechanism, at least for small slenderness values. It is also worth noting that Case 1 and Case 2 are two cases where tensile strength can be considered reasonably. However, Case 1 has a quite high cohesion, whereas in Case 2 cohesion is lower, more near to a NTM hypothesis with frictional behavior. Case 3 is characterized by very good cohesion, small but non-zero tensile strength and reasonable friction angle.

Table 3: Mechanical properties adopted for interfaces for different cases in MC simulations.

	τ_0 [MPa]	f_t [MPa]	Φ [Deg]
Case 1	0.10	$0.1\,\tau_0$	26
Case 2	0.05	$0.5\,\tau_0$	15
Case 3	0.2	$0.25\,\tau_0$	26

Results obtained with MC simulations for Case 1 are shown in Figure 15. In subfigures from –a to –c, the normalized collapse accelerations so obtained, i.e. $a_g / g = \min\{\lambda_1 \quad \dots \quad \lambda_5\}$, is plotted for each sampled tower against slenderness (Figure 15-a), tower height H (Figure 15-b) and normalized shear area (Figure 15-c).
Each sample is represented by a thick dot, with a color correspondent to the failure mechanism active, so that color yellow is used for Mechanism #1, blue #2, purple #3, green #4 and red #4.
As can be observed, MC results cumulate on well-defined areas of influence with different colors, which clearly indicate that different failure mechanisms are active for well-defined ranges of slenderness.
An interesting remark is that blue-failure mechanism (#2) is active only for large values of slenderness, meaning that the approach suggested by the Italian code may exhibit some strong limitations outside this range, because based on the activation of a failure mechanism which is improbable in reality. The determination of the active failure mechanism, indeed, appears particularly important in light of a possible strengthening intervention aimed at a vulnerability reduction.
The most probable failure mechanisms (observed in the majority of the cases) are either a “Heyman-type” collapse (with the formation of an inclined yield line) or a vertical splitting into two portions. Such outcome appears fully in agreement with post-earthquake surveys. Green failure mechanism, i.e. a combination of the previously mentioned two mechanisms clearly constitutes the smooth passage between vertical splitting and inclined rocking, in the region with smaller slenderness, probably because of the pure shear failure of the upper left portion of the tower.
Monolithic rocking at the base is possible (blue failure mechanism) but unlikely and occurs only for very large values of slenderness, which are also uncommon in practice.

Results obtained for Case 2 are synoptically depicted in Figure 16. In this particular situation, we are in presence of all the five failure mechanisms, with a strong reduction of the area where the inclined rocking (#3) is active, in favor of monolithic rocking (#2). Also, vertical splitting seems to become more probable, clearly providing normalized collapse accelerations lower than those obtained with Mechanism #2. Whilst in this case monolithic rocking appears more probable, the corresponding collapse acceleration is however always larger than that provided by Mechanism #1, so not on the safe size. It is also interesting to point out that the relatively small friction angle allows in this case a sliding failure (red Mechanism #5) which obviously occurs for towers exhibiting small slenderness.
It is interesting to notice that in the same figure results obtained with both the procedure proposed by the Italian code and UDEC are also represented. Thick black curve refers to the interpolation exponential formula found in the previous section assuming Italian code data, whereas dashed curves refer to UDEC results. Such curves are multiplied roughly by 4/3, because the distribution of horizontal loads adopted in MC limit analysis is constant, whereas for both UDEC and Italian code is reverse linear. It is also worth noting that Case 2 is the most adequate to compare with, because mechanical properties of the interfaces approximate a no tension material.
As can be observed, Italian code data (but UDEC as well in the majority of the cases) generally stand within the scatter area provided by MC simulations, but once again it is stressed how the active failure mechanism involves in the majority of the cases vertical shear cracks. UDEC trend is generally characterized by low collapse accelerations for large slenderness, with a deviation from MC scatter data. Italian code results seem to be less sensitive to slenderness, but the trend is conceptually similar. This feature can be justified by the role played by the assumption done in MC simulations of an infinite compressive strength, which can lead to an overestimation of the corresponding resisting bending moment on interfaces, see Eq. (2).
Finally, in Figure 17, the same results are replicated for Case 3, which seems to represent an intermediate situation between the previous two, where four of the five possible mechanisms are active. Again, green mechanism liaises with #1 and #3 and this appears pretty obvious being #2 a combination of them.
Blue mechanism, i.e. #2 (the one with the highest similarity with the Italian code) seems to increase its probability of occurrence, as shown by the extension of the blue scatter area. At least qualitatively, this last case seems the nearest to Italian code predictions, with a range of slenderness where rocking failure is possible much larger.
Again, the quantitative differences between Italian code prediction and present approach can be justified into the different formulas utilized to evaluate the ultimate bending moment (an approximate approach is adopted by the Italian code) and the adoption in the present investigation of non-null values for both tensile and tangential strength.
Data scatter seems larger in the last two cases, probably because of the possibility to activate more failure mechanisms (like the vertical splitting) that are quite sensible to a variation in the tower geometry and mechanical properties of the interfaces.
For Case 1, also FE upper bound limit analysis computations are performed on a sample of 100000 replicates, assuming for the interfaces the same failure criterion adopted in Figure 14-a. Results are summarized in Figure 18 in terms of a_g/g versus slenderness. A comparison with Italian code data and UDEC is also reported, in this case without multiplying fitting curves by 4/3 because in the FE limit analysis computations a reverse triangular distribution of horizontal loads is applied. The deviation on the collapse load at large values of slenderness can be again justified by the assumption of good mechanical properties for the interfaces with an infinite compressive strength.
As can be noted from the results, there is general agreement between MC FE limit analysis results and previously discussed approaches in terms of collapse acceleration, but again the variety of the failure mechanisms numerical found is much wider. For the sake of completeness, in Figure 18-b three different mechanisms (roughly corresponding to manual mechanisms 2, 3 and 4 evaluated previously) obtained with FE limit analysis at three slenderness values are represented. The limit analysis with FE exhibits a smooth transition between different mechanism and this feature is in

common with UDEC, which to some extent is able to fairly capture such variability, see Figure 7 and Figure 8.

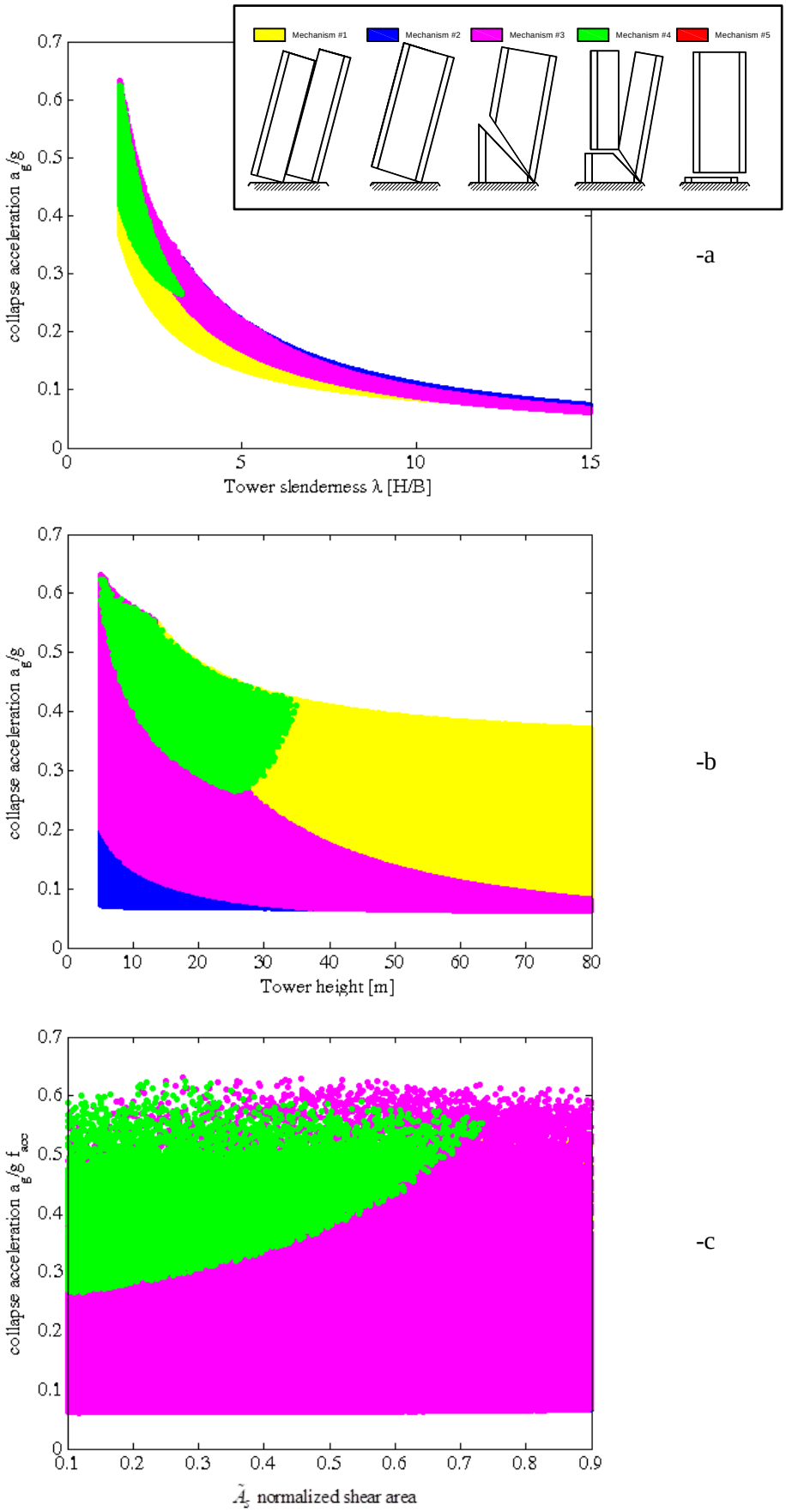

Figure 15: Case 1, Monte Carlo (5mln points) a_g/g diagrams and active mechanisms.

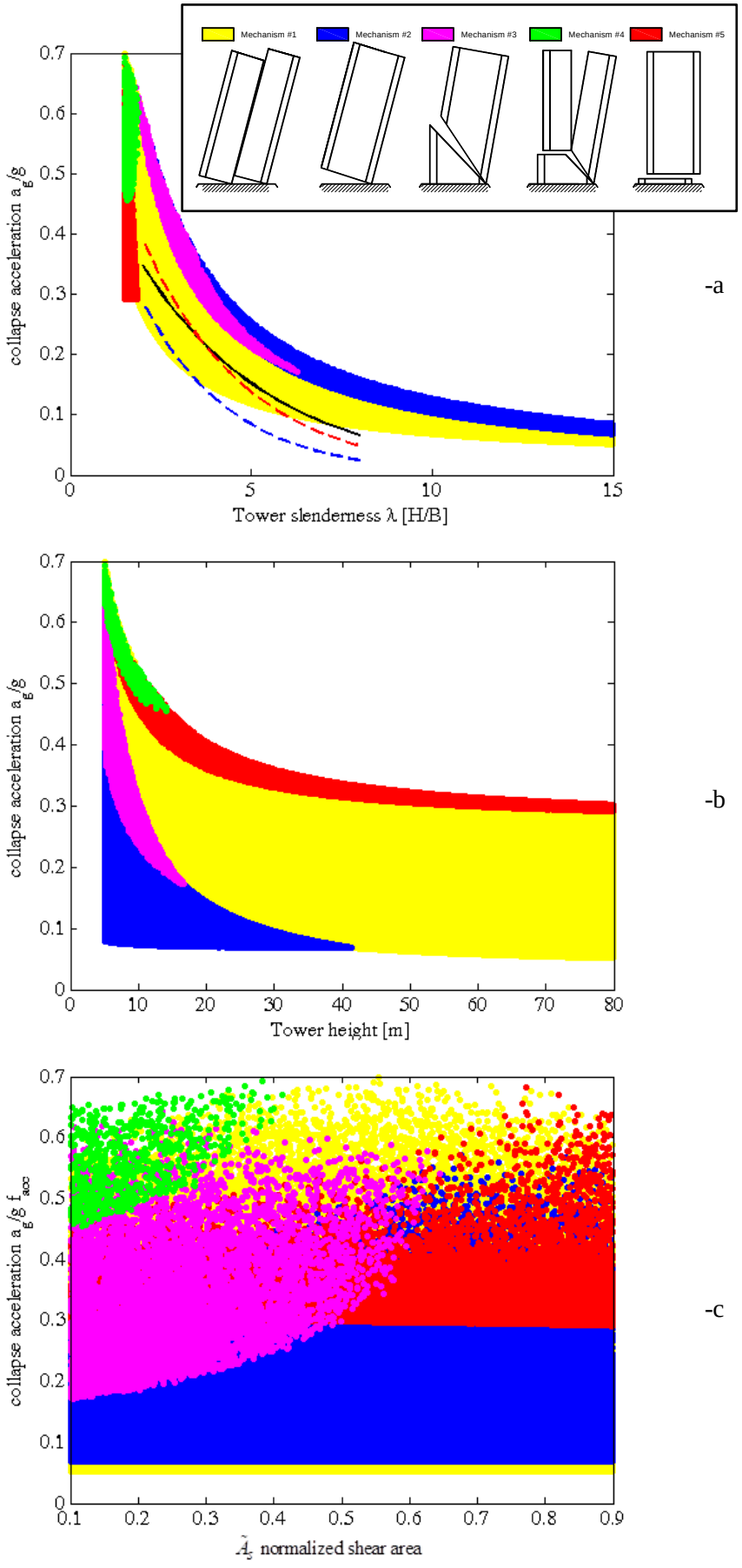

Figure 16: Case 2, Monte Carlo (5mln points) a_g/g diagrams and active mechanisms.

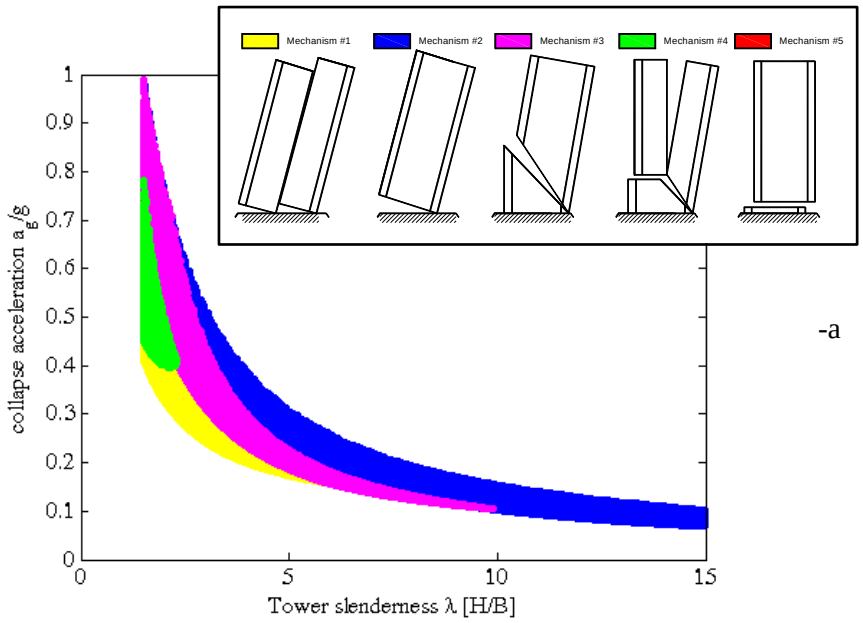

-a

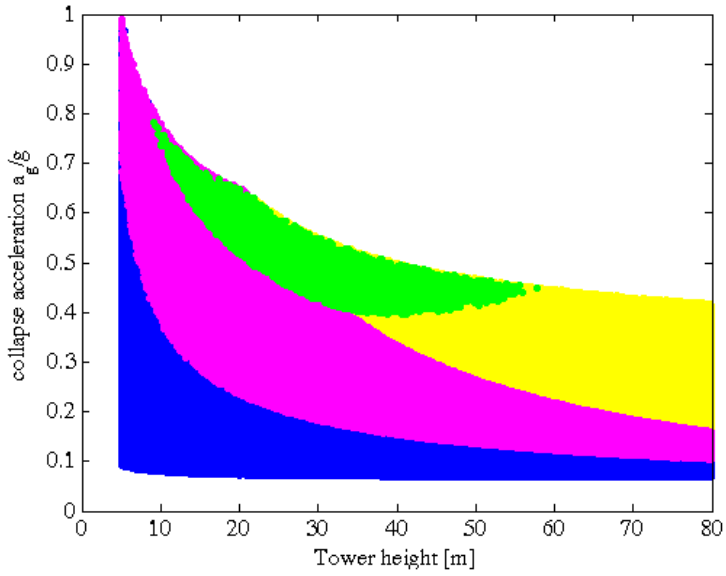

-b

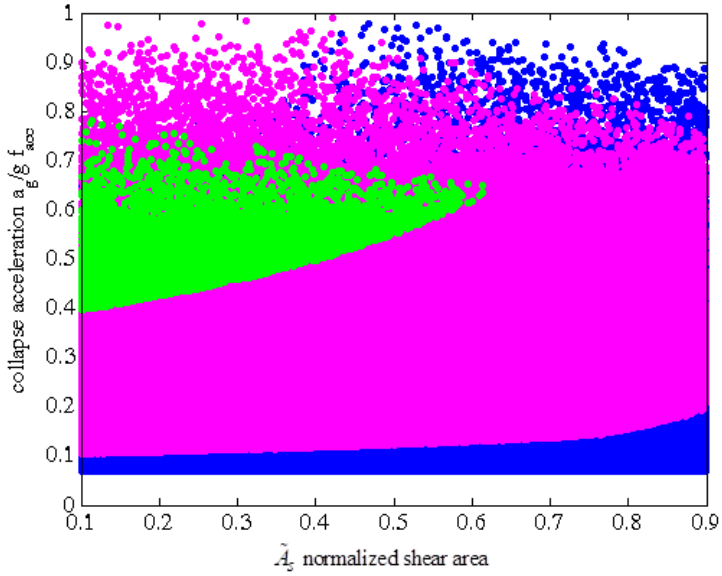

-c

Figure 17: Case 3, Monte Carlo (5mln points) a_g/g diagrams and active mechanisms.

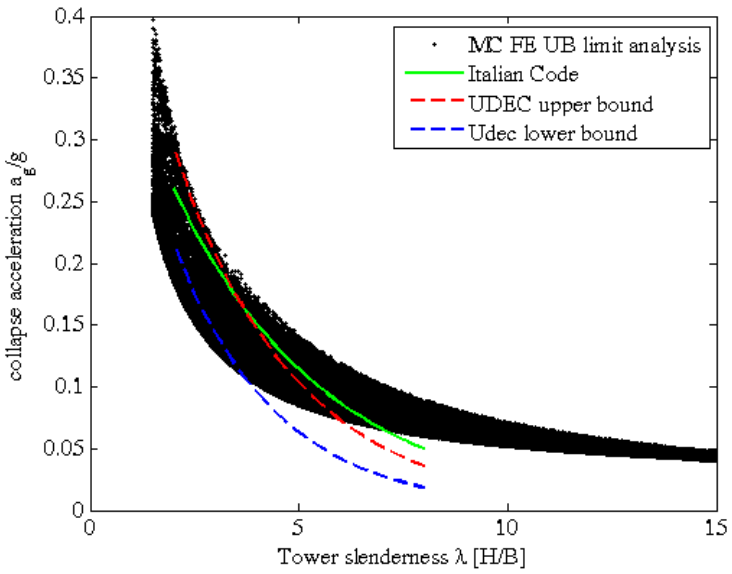

-a

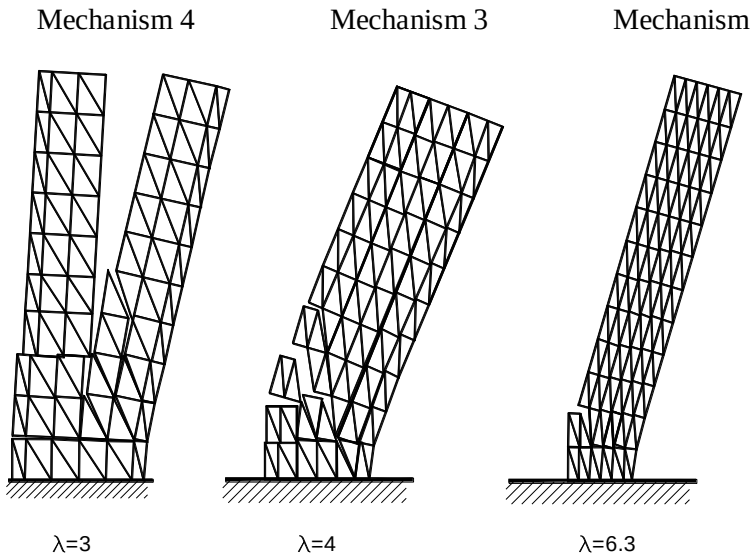

-b

Figure 18: Case 1, Monte Carlo simulations performed with the FE upper bound limit analysis approach.-a: a_g/g vs slenderness diagram. –b; some meaningful failure mechanisms found.

8 Comparison with real case-studies

One of the authors of this paper performed in the recent past different FE vulnerability analyses on 25 existing masonry towers located in the Northern Italy (Valente & Milani 2016a, 2016b, 2017). Partial results of the analysis are available in Valente & Milani (2016a**)** where the reader is referred for a full insight of the geometry and the numerical strategies adopted to evaluate the seismic vulnerability and hence the acceleration factors. In brief, the analyses where carried out using refined 3D FE discretizations within the commercial code ABAQUS (2006), assuming for masonry a sophisticated Concrete Damage Plasticity (CDP) model and performing non-linear static and dynamic simulations. By means of such approach, it was possible to evaluate the acceleration factor of each

tower and therefore such data can represent a valuable reference to eventually benchmark the results obtained with the simplified approaches here adopted. In Figure 19, Figure 20 and Figure 21 the acceleration factors found with Italian code approach, UDEC and 3Muri respectively are depicted against tower slenderness. The spectral ordinate corresponding to the fundamental period T_1 is here referred to a seismic zone Z_1 by EC8 with soil D. Italian code is not utilized in this case because the spectrum is given there only knowing the latitude and longitude of tower location instead giving distinct seismic zones.

For the sake of comparison, the acceleration factors of the aforementioned 25 real towers are also represented using green diamonds.

As can be noted, the vulnerability of the real 25 towers is generally well predicted by the fitting curves provided by all models. Italian Guidelines curve slightly overestimates the acceleration factor, clearly because it does not take into account the presence of irregularities.

However, once again and for the reasons previously discussed, the variability of the failure mechanisms is totally lost in both Italian code and 3Muri, whereas only UDEC seems able to reproduce –despite roughly- vertical splitting and rocking at the base. In Figure 22 the results in terms of damage patterns (red: full damage, blue: no damage) obtained in ABAQUS for 6 of the 25 real towers studied are depicted with the aim of having an insight into the different failure mechanisms active. As can be observed, towers are ordered from the left to the right at increasing slenderness. In general, the transition is consistent with MC results obtained with pre-assigned mechanisms (see Figure 16), so that a small slenderness favors a sliding at the base and then, smoothly all the other mechanisms become active, ending with the vertical splitting that is observed for moderate/high slenderness values.

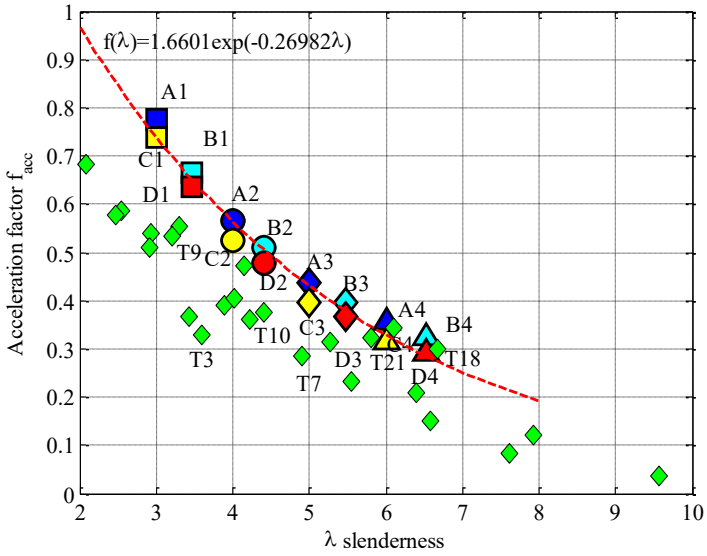

Figure 19: Italian Guidelines for the Built Heritage. Acceleration factor vs slenderness, comparison between idealized approach and real case studies.

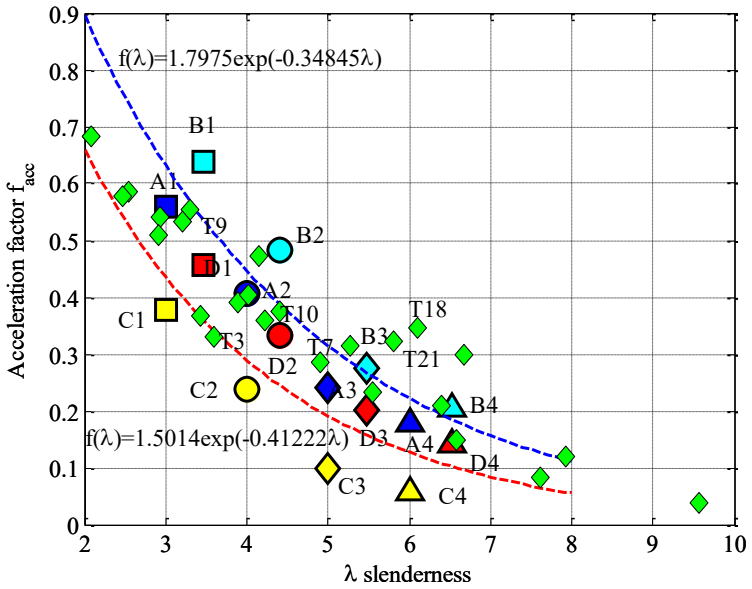

Figure 20: UDEC software. Acceleration factor vs slenderness, comparison between idealized approach and real case studies.

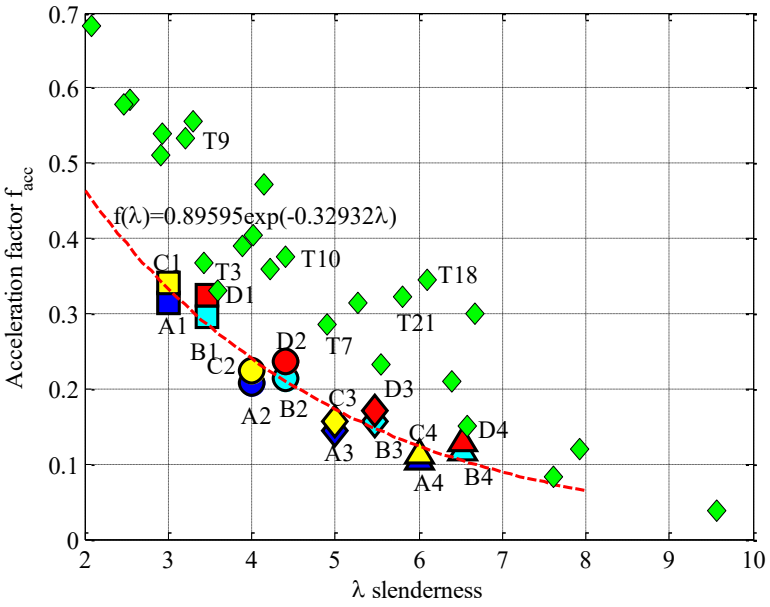

Figure 21: 3Muri software. Acceleration factor vs slenderness, comparison between idealized approach and real case studies.

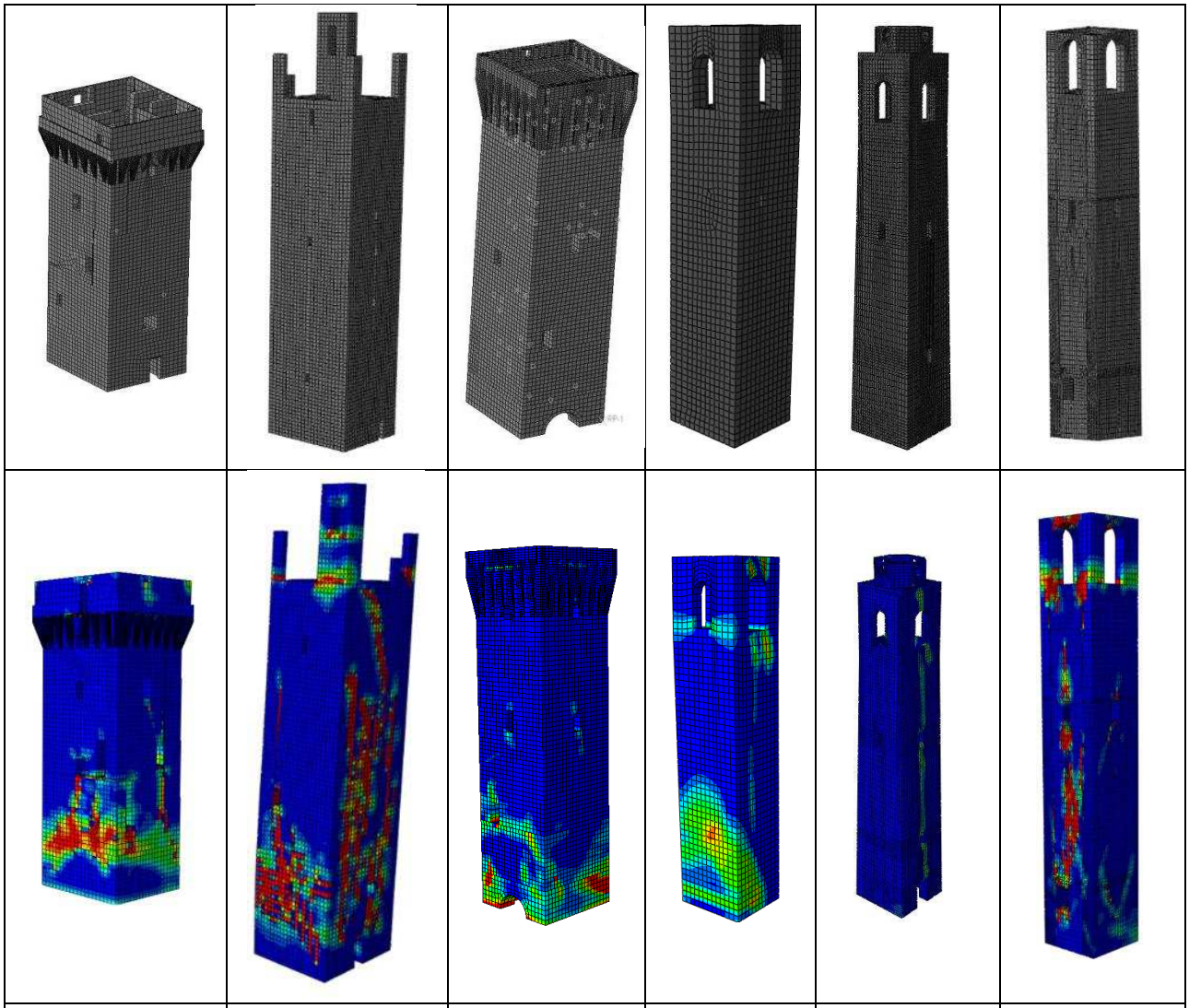

Mechanism #5	Mechanism #4	Mechanism #2	Mechanism #3	Mechanism #1	Mechanism #1/2
$\lambda = \mathbf{3.2}$ **T9**	$\lambda = \mathbf{3.6}$ **T3**	$\lambda = \mathbf{4.4}$ **T10**	$\lambda = \mathbf{4.9}$ **T7**	$\lambda = \mathbf{5.8}$ **T21**	$\lambda = \mathbf{6.1}$ **T18**

Figure 22: Damage patterns (red: full damage, blue: no damage) obtained in Abaqus for 6 real size and configuration towers in order of increasing slenderness.

9 Conclusions

We have presented several different simplified approaches to roughly predict, without needing any calculation, an estimation of collapse acceleration and associated active failure mechanism of masonry towers subjected to seismic excitation. The approaches used rely into (1) a simplified approach by Italian Code, (2) UDEC, (3) 3Muri and (4) an upper bound limit analysis performed either with pre-assigned failure mechanisms or FEs. The procedure is applied on idealized towers, geometrically regular (without openings, bell cells and internal vaults) exhibiting variable height, cross shear area and slenderness. By means of the application of models (1) - (3) on 16 idealized towers we presented simplified fitting formulas to predict, without any computation, the collapse acceleration and acceleration factor of any existing tower as a function of slenderness. Model (4)

allowed performing large scale Monte Carlo simulations, showing how different failure mechanisms can take place in dependence of the geometrical features of the structures.

The results have been also benchmarked using previously presented vulnerability studies conducted on 25 real case-studies, showing a satisfactory agreement.

The comparative study however puts in evidence how Italian Code, which bases on the assumption of failure for the formation of a flexural hinge (in this case at the base thanks to the regularity of the examples treated) provides collapse accelerations generally on the safe side, but with a possibly wrong failure mechanism. This limitation appears particularly important in light of a strengthening intervention, where the knowledge of the crack pattern is mandatory. UDEC on the contrary, despite roughly, seems to provide more accurate mechanisms to be used for practical purposes.

Finally, in UDEC an important question arises on the choice of the optimal mesh. In order to be effective, indeed, UDEC (like any other DEM code available in the market) would require that the edges of the blocks preferentially coincide with the active crack patterns. In the simulations performed in the present paper, it has been shown that the active failure mechanism involves only vertical and horizontal yield lines, therefore a rectangular discretization is perfectly adequate. When Mechanisms #3 and #4 are active, i.e. when failure involves some inclined yield lines, a regular pattern of blocks still adapts reasonably well, because the inelastic deformation zigzags around the real inclined crack. If the refinement is relatively high (even medium meshes proved to be effective), the approximation turns into a slight overestimation of the load carrying capacity, which can be considered fully acceptable for practical purposes.

References

ABAQUS®, Theory Manual, Version 6.14, 2006.

Acito M., M. Bocciarelli, C. Chesi, G. Milani, Collapse of the clock tower in Finale Emilia after the May 2012 Emilia Romagna earthquake sequence: Numerical insight. Engineering Structures, **72**, 70-91, 2014.

Bayraktar A., A. Sahin, M. Özcan, F. Yildirim, Numerical damage assessment of Haghia Sophia bell tower by nonlinear FE modeling. Applied Mathematical Modelling, **34**, 92–121, 2010.

Bernardeschi K., C. Padovani, G. Pasquinelli, Numerical modelling of the structural behaviour of Buti's bell tower. Journal of Cultural Heritage, **5**, 371–378, 2004.

Bui T.T., A. Limam, V. Sarhosis, M. Hjiaj, Discrete element modelling of the in-plane and out-of-plane behaviour of dry-joint masonry wall constructions. Engineering Structures, **136**, 277-294, 2017.

Carpinteri A., S. Invernizzi, G. Lacidogna, Numerical assessment of three medieval masonry towers subjected to different loading conditions. Masonry International, **19**, 65–75, 2006.

Casolo S., G. Milani, G. Uva, C. Alessandri, Comparative seismic vulnerability analysis on ten masonry towers in the coastal Po Valley in Italy. Engineering Structures, **49**, 465-490, 2013.

Circolare n° 617 del 2 febbraio 2009. Istruzioni per l'applicazione delle nuove norme tecniche per le costruzioni di cui al decreto ministeriale 14 gennaio 2008. [Instructions for the application of the new technical norms on constructions].

Como M., Statics of Historic Masonry Constructions, Springer, 2013

Cundall P.A. A computer model for simulating progressive, large-scale movements in blocky rock systems. In: Proceedings of the International Symposium on Rock Mechanics, Nancy, France, 129–136, 1971.

Curti E., S. Lagomarsino, S. Podestà, Dynamic models for the seismic analysis of ancient bell towers. In Proc.: Lourenço PB, Roca P, Modena C, Agrawal S (Eds.), Structural Analysis of Historical Constructions SAHC-2006, MacMillan, New Delhi, India.

DPCM 9/2/2011. Linee guida per la valutazione e la riduzione del rischio sismico del patrimonio culturale con riferimento alle Norme tecniche delle costruzioni di cui al decreto del Ministero delle Infrastrutture e dei trasporti del 14 gennaio 2008. [Italian guidelines for the evaluation and the reduction of the seismic risk for the built heritage, with reference to the Italian norm of constructions].

EC8. EN 1998-3, Eurocode 8: Design of structures for earthquake resistance – Part 3: Assessment and retrofitting of buildings. European Committee for Standardization, Brussels, Belgium, 2005.

Fabbrocino F., Estimation of the natural periods of existing masonry towers through empirical procedure. International Journal of Sustainable Materials and Structural Systems, **2**(3-4), 250 –261, 2016.

Forgacs T., Sarhosis V., Bagi K., Minimum thickness of semi-circular skewed masonry arches. Engineering Structures, **140**, 317–336, 2017.

Formisano A., Vituat. R., Milani G., Sarhosis V., Parametric seismic analysis on masonry bell towers. In Proc. ANIDIS 2017, XVII Congress of the Italian Association of Seismic Engineering. Pistoia, Italy, 17-21 September 2017, 2017.

Galasco A., S. Lagomarsino, Penna A., TREMURI Program: Seismic Analyser of 3D Masonry Buildings, University of Genoa, Italy, 2002.

Heyman J., The stone skeleton, Cambridge University Press, 1995.

ITASCA: UDEC – Universal Distinct Elements Code Manual. Theory and Background, Itasca consulting group, Minneapolis, USA, 2004.

Lagomarsino S., Penna A., Galasco A., Cattari S. TREMURI Program: An equivalent frame model for the nonlinear seismic analysis of masonry buildings. Engineering Structures, **56**, 1787-1799, 2013.

Lubliner J., J. Oliver, S. Oller, E.A. Onate, A plastic-damage model for concrete. International Journal of Solids and Structures, **25**(3), 299-326, 1989.

Milani G., R. Shehu, M. Valente, Role of inclination in the seismic vulnerability of bell towers: FE models and simplified approaches, Bulletin of Earthquake Engineering, **15**(4), 1707-1737, 2017.

Milani G., S. Casolo, A. Naliato, A. Tralli, Seismic assessment of a medieval masonry tower in Northern Italy by limit, nonlinear static, and full dynamic analyses. International Journal of Architectural Heritage, **6** (5), 489-524, 2012a.

Milani G., Lourenço P.B., Tralli A, Homogenised limit analysis of masonry walls, Part I: Failure surface. Computers & Structures, **84**(3-4), 166-180, 2006a.

Milani G., P.B. Lourenço, A. Tralli, Homogenised limit analysis of masonry walls, Part II: Structural examples. Computers & Structures, **84**(3-4), 181-195, 2006b.

Milani G., S. Russo, M. Pizzolato, A. Tralli, Seismic behavior of the San Pietro di Coppito church bell tower in L'Aquila, Italy, The Open Civil Engineering Journal, **6** (Sp. Issue #1), 131-147, 2012b.

NTC 2008 Decreto Ministeriale 14/1/2008. Norme tecniche per le costruzioni, Ministry of Infrastructures and Transportations. G.U. S.O. n.30 on 4/2/2008; 2008 (in Italian)

Peña F., P.B. Lourenço, N. Mendez, D. Oliveira, Numerical models for the seismic assessment of an old masonry tower. Engineering Structures, **32**, 1466-1478, 2010.

Pulatsu B., Sarhosis V., Bretas E. Lourenco P. Nikitas N. Nonlinear static behavior of multi-drum ancient columns. Structures and Buildings, **1**(1), 1-13, 2017.

Riva P., F. Perotti, E. Guidoboni, E. Boschi. Seismic analysis of the Asinelli Tower and earthquakes in Bologna. Soil Dynamics and Earthquake Engineering, **17**, 525–550, 1998.

S.T.A.DATA. 3Muri. Seismic calculation of masonry structures according to the Italian Ministerial Decree 14/01/2008 "New technical codes for constructions", 2016.

Sarhosis V., D.V. Oliveira, J.V. Lemos, P.B. Lourenco, The effect of skew angle on the mechanical behaviour of masonry arches. Mech Res Commun, **61**, 53–59, 2014.

Sarhosis V., P. Asteris, T. Wang, W. Hu, Y. Han (2016b). On the stability of ancient colonnades under static and dynamic conditions, Bulletin of Earthquake Engineering, 1-22, DOI 10.1007/s10518-016-9881-z.V.

Sarhosis, K. Bagi, J.V. Lemos, G. Milani, Computational modelling of masonry structures using the discrete element method. USA: IGI Global, 2016. DOI: 10.4018/978-1-5225-0231-9

Sarhosis V., Garrity S.W., Sheng Y., Influence of brick–mortar interface on the mechanical behaviour of low bond strength masonry brickwork lintels. Eng Struct, **88**, 1–11, 2015.

Sarhosis V., Sheng Y., Identification of material parameters for low bond strength masonry, Engineering Structures, **60**, 100-110, 2014. DOI: 10.1016/j.engstruct.2013.12.013.

Valente M., G. Milani, Effects of geometrical features on the seismic response of historical masonry towers. Journal of Earthquake Engineering, in press, 2017.

Valente M., G. Milani, Non-linear dynamic and static analyses on eight historical masonry towers in the North-East of Italy. Engineering Structures, **114**, 241–270, 2016a.

Valente M., G. Milani, Seismic assessment of historical masonry towers by means of simplified approaches and standard FEM. Construction and Building Materials, **108**, 74–104, 2016b.